Shear Wave Logging In (Multilayered) Elastic Formations: An Overview

by

D.P. Schmitt and C.H. Cheng

Earth Resources Laboratory
Department of Earth, Atmospheric, and Planetary Sciences
Massachusetts Institute of Technology
Cambridge, MA 02139

ABSTRACT

We perform the analysis of the dispersion and attenuation of the modes generated both by a dipole and quadrupole source in a fluid filled borehole surrounded by a (multilayered) elastic formation. The displacement-stress vectors are propagated through the layers using the Thomson-Haskell method. Only the well bonded configuration is investigated. In the time domain, we investigate the effects of the source center frequency on synthetic full waveform microseismograms computed using the discrete wavenumber method.

Whatever the formation (fast or slow) and the configuration, the low frequency part of both the flexural and screw modes follows the virgin formation shear wave characteristics. Their high frequency parts behave like that of the Stoneley wave excited by a monopole source. As a result, the fundamental modes are very sensitive to the properties of the inner layers at intermediate and high frequencies. In the presence of an invaded zone, the internal dynamics of the waveforms can be significantly modified, while the useful starting energy of the fundamental modes is shifted toward lower frequencies. The reverse phenomenon occurs when the borehole is cased. For this last configuration, it is only with low source center frequencies that multipole sources can log a slow formation shear wave due to the leaky character of the fundamental modes.

INTRODUCTION

Detailed lithological identification requires the evaluation of both P- and S-wave velocities and attenuations. The shear wave characteristics can be extracted from the conventionnal axisymmetric (monopole) tool recorded wavetrains through a critically refracted S wave or the low frequency part of the first pseudo-Rayleigh mode. This is possible only when the formation shear velocity is greater than the acoustic velocity of the borehole fluid, i.e., in the presence of a so called fast formation. In the presence of a "slow" formation, Stoneley wave characterisitics may be used although the results will be much more questionable, especially in porous formations of high permeability. These limitations have motivated the design of logging tools which will provide this information whatever the formation veocities (White, 1967; Kitsunezaki, 1980; Benzing and Endres, 1983; Zemanek et al., 1984; Chen, 1984, 1985).

Theoretical investigations have been performed by several authors in the presence of radially semi-infinite pure elastic formations. Roever et al. (1974), Winbow and Rice (1984) and Winbow (1985) considered off-axis volume source and receiver. Tongtaow (1982) considered point force and the presence of a tool at the center of the well bore as well as transversely isotropic formations. Kurkjian and Chang (1986) derived the expressions of a multipole point source. Kurkjian (1986) studied the low frequency radiation of a horizontal point force compared with a dipole excitation and analyzed the borehole related effects. The multilayered formation situation has been less extensively studied. Baker and Winbow (1985) studied the depth of penetration of both P and S waves generated by dipole and quadrupole sources in the presence of an invaded zone. Everhart and Chang (1985) displayed synthetic microseismograms obtained with a dipole source in a cased hole both for the well bonded and the so called free pipe situations.

In this paper, we consider dipole and quadrupole *point* sources, following Kurkjian and Chang (1986). In the first part, we briefly review the theoretical formulation and extend it to the well bonded multilayered configuration using the Thomson-Haskell method. Considering both slow and fast formations, we analyze the dispersion and attenuation of the generated modes, essentially the flexural and screw modes. Several situations are investigated such as radially semi-infinite formations, the presence of an invaded zone, and well bonded cased holes. Full waveform synthetic microseismograms computed using the discrete wavenumber method are also displayed for various source center frequencies.

THEORETICAL BACKGROUND

Configuration

We define a cylindrical coordinate system as (r, θ, z). The model consists of a fluid-fluid borehole, extending to infinity in the z direction, embedded in an elastic medium. The surrounding formation is composed of N concentric elastic layers. The radii R_{j-1} and R_j bound the j-th layer, the N-th one being radially semi-infinite. The borehole fluid layer is denoted by the index 1. Each layer is characterized by its P-wave velocity α_j, its S-wave velocity β_j and its density ρ_j. An anelastic attenuation characterized by quality factors Q_{α_j} and Q_{β_j} can be assumed in each shell. It implies a velocity dispersion. Considering a temporal dependence of the form $e^{-i\omega t}$, each velocity becomes (e.g., Aki and Richards, 1980):

$$c(\omega) = \frac{c(\omega_0)}{\left\{1 + \frac{1}{\pi Q} \ln \frac{\omega_0}{\omega}\right\}\left\{1 + \frac{i}{2Q}\right\}} \tag{1}$$

where

$c(\omega_0)$ = reference velocity (α_j, β_j) at the angular frequency ω_0,

$c(\omega)$ = velocity $(\alpha_j(\omega), \beta_j(\omega))$ at the angular frequency ω,

Q = quality factor $(Q_{\alpha_j}, Q_{\beta_j})$.

Source formulation and solution for the bore fluid

The potential $\tilde{\Phi}$ of a monochromatic point source located at (R_0, θ_0, z_0), in a fluid medium whose velocity is α_1, is the solution of the equation:

$$\frac{\partial^2 \tilde{\Phi}}{\partial t^2} - \alpha_1^2 \nabla^2 \tilde{\Phi} = 4\pi^2 \alpha_1^2 \delta(Z) e^{-i\omega t} \tag{2}$$

where

∇^2 denotes the Laplacian operator,

$Z = \left(r^2 + R_0^2 - 2rR_0 \cos(\theta - \theta_0) + (z - z_0)^2\right)^{\frac{1}{2}}$

ω is the angular frequency.

The solution of this equation is:

$$\tilde{\Phi} = \frac{1}{Z} e^{i\frac{\omega Z}{\alpha_1}} e^{-i\omega t} \tag{3}$$

which can be expressed as the superposition of cylindrical waves (Gradshteyn and Rhyzhik, 1965):

$$\tilde{\Phi} = \frac{e^{-i\omega t}}{\pi} \int_{-\infty}^{+\infty} K_0 \left\{ kp_1 (r^2 + R_0^2 - 2rR_0 \cos(\theta - \theta_0))^{\frac{1}{2}} \right\} e^{ik(z-z_0)} dk \tag{4}$$

where

$kp_1^2 = k^2 - \omega^2/\alpha_1^2$ is the radial wavenumber, k being the axial wavenumber.

K_0 is the modified Bessel function of the second kind of the zeroth order.

Using the Bessel function addition theorem (Watson, 1922), one obtains for $r > R_0$:

$$\tilde{\Phi} = \frac{e^{-i\omega t}}{\pi} \int_{-\infty}^{+\infty} \sum_{n=0}^{+\infty} \varepsilon_n \cos[n(\theta - \theta_0)] I_n(kp_1 R_0) K_n(kp_1 r) e^{ik(z-z_0)} dk \tag{5}$$

and, for $r < R_0$:

$$\tilde{\Phi} = \frac{e^{-i\omega t}}{\pi} \int_{-\infty}^{+\infty} \sum_{n=0}^{+\infty} \varepsilon_n \cos[n(\theta - \theta_0)] I_n(kp_1 r) K_n(kp_1 R_0) e^{ik(z-z_0)} dk \tag{6}$$

In the above expresions, I_n denotes the modified Bessel functions of the first kind of the nth order, while $\varepsilon_n = 2 - \delta_{n0}$ is the Neumann's factor. These formulae are identical to the ones given by Roever et al. (1974), Winbow (1985), Kurkjian and Chang (1986) and Kurkjian (1986).

Following Kurkjian and Chang (1986), a multipole source of order n is constructed by considering $2n$ monopoles in the same horizontal plane. They are distributed periodically along a circle of radius R_0 and alternate in sign (see Figure 2 of Kurkjian and Chang, 1986). The j-th point has a sign of $(-1)^{j+1}$, a scaling factor of $1/2n$ and is located at an angle of $[\pi(j-1)/n] + \xi$, relative to some reference, where $j = 1, ..., 2n$. The resulting potential in the frequency-axial wavenumber domain may then be written:

$$\Phi = e^{ikz} e^{-i\omega t} \sum_{j=1}^{+\infty} I_{(2j-1)n}(kp_1 R_0) \varepsilon_{(2j-1)n} K_{(2j-1)n}(kp_1 R_0) \cos[(2j-1)n(\theta - \xi)] \tag{7}$$

Considering a multipole *point source*, R_0 tends to zero. Using only the first term of the limited development of the Bessel function of the first kind of the n-th order (Abramovitz

and Stegun, 1965), which corresponds to the main contributor to the wavefield in the space-time domain, the potential of such a source is then given by:

$$\Phi^{(n)} = \frac{\varepsilon_n}{2^n n!}(kp_1 R_0)^n K_n(kp_1 R_0)\cos[n(\theta-\xi)]e^{ikz}e^{-i\omega t} \tag{8}$$

The total wavefield in the borehole fluid corresponds to the sum of the source contribution (characterized by $\Phi^{(n)}$) and the reflected wavefield. The radiation conditions prescribe that this last remains finite at the axis of the borehole. The expression of the associated displacement potential with respect to a n-th order multipole point source is given in the frequency-axial wavenumber domain by:

$$\Phi_1^{(n)} = \frac{1}{n!}\left(\frac{kp_1 R_0}{2}\right)^n \tilde{A_1}^{(n)} I_n(kp_1 r)\cos[n(\theta-\xi)]e^{ikz}e^{-i\omega t} \tag{9}$$

where $\tilde{A_1}^{(n)}$ is a function of k and ω.

The associated radial displacement $u(n,\,1,\,r)$ and stress $\sigma_{rr}(n,\,1,\,r)$ are:

$$\begin{cases} u(n,\,1,\,r) &= \dfrac{\partial\tilde{\Phi}_1^{(n)}}{\partial r} \\ \sigma_{rr}(n,\,1,\,r) &= -\rho_1\omega^2\tilde{\Phi}_1^{(n)} \end{cases} \tag{10}$$

Solutions for the elastic layers

The displacement vector in the j-th layer $\vec{u}(j,\,r) = (u(j,\,r)\,, v(j,\,r)\,w(j,\,r))^T$ may be expressed as:

$$\vec{u}(j,\,r) = \nabla\Phi_j + \nabla\times(\chi_j\vec{z}) + \nabla\times\nabla\times(\Gamma_j\vec{z}) \tag{11}$$

where

- Φ_j is the compressional wave potential,
- $\vec{z}$ is the unit vector in the z direction,
- Γ_j is the vertically polarized shear wave potential (SV),
- χ_j is the horizontally polarized shear wave potential (SH).

Each of these potentials is the solution of a scalar (Helmholtz) wave equation:

$$\begin{cases} \nabla^2\Phi_j + \dfrac{\omega^2}{\alpha_j^2}\Phi_j &= 0 \\ \nabla^2\chi_j + \dfrac{\omega^2}{\beta_j^2}\chi_j &= 0 \\ \nabla^2\Gamma_j + \dfrac{\omega^2}{\beta_j^2}\Gamma_j &= 0 \end{cases} \tag{12}$$

where ∇^2 is the Laplacian operator:

$$\nabla^2 = \frac{\partial^2}{\partial r^2} + \frac{1}{r}\frac{\partial}{\partial r} + \frac{1}{r^2}\frac{\partial^2}{\partial \theta^2} + \frac{\partial^2}{\partial z^2} \tag{13}$$

Analogous to the borehole fluid, the displacement potentials, with respect to a n-th order multipole, may be expressed in each elastic shell as:

$$\begin{cases} \Phi_j^{(n)} &= e^{-i\omega t}e^{ikz}\dfrac{1}{n!}\left(\dfrac{kp_1\,R_0}{2}\right)^n \{A_{nj}I_n(kp_j\,r) + B_{nj}K_n(kp_j\,r)\}\cos[n(\theta-\xi)] \\ \chi_j^{(n)} &= e^{-i\omega t}e^{ikz}\dfrac{1}{n!}\left(\dfrac{kp_1\,R_0}{2}\right)^n \{C_{nj}I_n(ks_j\,r) + D_{nj}K_n(ks_j\,r)\}\sin[n(\theta-\xi)] \\ \Gamma_j^{(n)} &= e^{-i\omega t}e^{ikz}\dfrac{1}{n!}\left(\dfrac{kp_1\,R_0}{2}\right)^n \{E_{nj}I_n(ks_j\,r) + F_{nj}K_n(ks_j\,r)\}\cos[n(\theta-\xi)] \end{cases} \tag{14}$$

where

- I_n and K_n denote the first and second kind modified Bessel functions of the n-th order,
- $kp_j^2 = k^2 - \omega^2/\alpha_j^2$ and $ks_j^2 = k^2 - \omega^2/\beta_j^2$ are the radial wavenumbers,
- A_{nj}, B_{nj}, C_{nj}, D_{nj}, E_{nj} and F_{nj} are functions of the axial wavenumber k and the angular frequency ω.

The radiation conditions imply that $A_{nN} = C_{nN} = E_{nN} = 0$.

In terms of potentials, the displacements are:

$$\begin{cases} u(n,\,j,\,r) &= \dfrac{\partial\Phi_j^{(n)}}{\partial r} + \dfrac{1}{r}\dfrac{\partial\chi_j^{(n)}}{\partial\theta} + \dfrac{\partial^2\Gamma_j^{(n)}}{\partial r\partial z} \\ v(n,\,j,\,r) &= \dfrac{1}{r}\dfrac{\partial\Phi_j^{(n)}}{\partial\theta} - \dfrac{\partial\chi_j^{(n)}}{\partial r} + \dfrac{1}{r}\dfrac{\partial^2\Gamma_j^{(n)}}{\partial\theta\partial z} \\ w(n,\,j,\,r) &= \dfrac{\partial\Phi_j^{(n)}}{\partial z} + \dfrac{\omega^2}{\beta_j^2}\Gamma_j^{(n)} + \dfrac{\partial^2\Gamma_j^{(n)}}{\partial z^2} \end{cases} \tag{15}$$

The elements e_{ij} of the strain tensor are:

$$\left\{\begin{array}{rcl} e_{rr}(n,\,j,\,r) & = & \dfrac{\partial u(n,\,j,\,r)}{\partial r} \\ e_{\theta\theta}(n,\,j,\,r) & = & \dfrac{u(n,\,j,\,r)}{r} + \dfrac{1}{r}\dfrac{\partial v(n,\,j,\,r)}{\partial \theta} \\ e_{zz}(n,\,j,\,r) & = & \dfrac{\partial w(n,\,j,\,r)}{\partial z} \\ e_{r\theta}(n,\,j,\,r) & = & \dfrac{1}{2}\left\{\dfrac{1}{r}\dfrac{\partial u(n,\,j,\,r)}{\partial \theta} - \dfrac{1}{r}v(n,\,j,\,r) + \dfrac{\partial v(n,\,j,\,r)}{\partial r}\right\} \\ e_{\theta z}(n,\,j,\,r) & = & \dfrac{1}{2}\left\{\dfrac{1}{r}\dfrac{\partial w(n,\,j,\,r)}{\partial \theta} + \dfrac{\partial v(n,\,j,\,r)}{\partial z}\right\} \\ e_{rz}(n,\,j,\,r) & = & \dfrac{1}{2}\left\{\dfrac{\partial w(n,\,j,\,r)}{\partial r} + \dfrac{\partial u(n,\,j,\,r)}{\partial z}\right\} \end{array}\right. \tag{16}$$

while the stress-strain relation are classically given by:

$$\sigma_{ij}(n,\,j,\,r) = \lambda_j e(n,\,j,\,r)\delta_{ij} + 2\mu_j e_{ij}(n,\,j,\,r) \tag{17}$$

where

- $\lambda_j = \rho_j(\alpha_j^2 - 2\beta_j^2)$ is the Lamé coefficient of the layer,
- $e(n,\,j,\,r) = e_{ii}(n,\,j,\,r) = -\omega^2\Phi_j^{(n)}/\alpha_j^2$ is the dilatation,
- δ_{ij} is the Kronecker delta (i.e. the unit tensor),
- $\mu_j = \rho_j\beta_j^2$ is the shear modulus of the layer.

For the j-th layer, the relations (15) and (17) may be written in a matrix form:

$$\underline{\mathbf{S}}(n,\,j,\,r) = \underline{\underline{\mathbf{T}}}(n,\,j,\,r)\underline{\mathbf{X}}_{n,j} \tag{18}$$

where

n denotes the order of the source considered,

$\underline{\mathbf{S}}(n,\,j,\,r) = (u(n,j,r),\, v(n,j,r),\, w(n,j,r), \sigma_{rr}(n,j,r,),\, \sigma_{r\theta}(n,j,r),\, \sigma_{rz}(n,j,r))^T$ is the displacement-stress vector,

$\underline{\mathbf{X}}_{n,j} = (A_{nj},\, B_{nj},\, C_{nj},\, D_{nj},\, E_{nj},\, F_{nj})^T$

$\underline{\underline{\mathbf{T}}}(n,\,j,\,r)$ is a 6x6 complex matrix whose elements are given in the Appendix.

Continuity equations and propagation

At each solid-solid interface (i.e., at R_j between the j-th and (j+1)-th layer, with j= 2,.....,N-1), the boundary conditions ensuring the unicity of the wavefield (Neumann's theorem), assuming a welded contact, are:

$$\begin{cases} 1)\ u(n,\, j,\, R_j) &= u(n,\, j+1,\, R_j) \\ 2)\ v(n,\, j,\, R_j) &= v(n,\, j+1,\, R_j) \\ 3)\ w(n,\, j,\, R_j) &= w(n,\, j+1,\, R_j) \\ 4)\ \sigma_{rr}(n,\, j,\, R_j) &= \sigma_{rr}(n,\, j+1,\, R_j) \\ 5)\ \sigma_{r\theta}(n,\, j,\, R_j) &= \sigma_{r\theta}(n,\, j+1,\, R_j) \\ 6)\ \sigma_{rz}(n,\, j,\, R_j) &= \sigma_{rz}(n,\, j+1,\, R_j) \end{cases} \tag{19}$$

In order to propagate the displacement-stress vectors through the layers and so to determine the weighting coefficients, the Thomson-Haskell method is used.

For j=1,.....,$N-2$, the boundary conditions at $r = R_{N-j}$ may be written :

$$\underline{\mathbf{S}}(n,\, N-j,\, R_{N-j}) = \underline{\underline{\mathbf{T}}}(n,\, N-j,\, R_{N-j})\underline{\mathbf{X}}_{n,N-j} \tag{20}$$

while at $r = R_{N-j-1}$, for j=0,.....,$N-2$, one obtains:

$$\underline{\mathbf{S}}(n,\, N-j,\, R_{N-j-1}) = \underline{\underline{\mathbf{T}}}(n,\, N-j,\, R_{N-j-1})\underline{\mathbf{X}}_{n,N-j} \tag{21}$$

From the above two latter equations, one can deduce, for j=1,....,$N-2$:

$$\underline{\mathbf{S}}(n,\, N-j,\, R_{N-j}) = \underline{\underline{\mathbf{T}}}(n,\, N-j,\, R_{N-j})\underline{\underline{\mathbf{T}}}^{-1}(n,\, N-j,\, R_{N-j-1})\underline{\mathbf{S}}(n,\, N-j,\, R_{N-j-1}) \tag{22}$$

At the different interfaces, the continuity equations may be written for j=0,....,$N-2$:

$$\underline{\mathbf{S}}(n,\, N-j,\, R_{N-j-1}) = \underline{\mathbf{S}}(n,\, N-j-1,\, R_{N-j-1}) \tag{23}$$

The equations (22) and (23) finally lead to:

$$\underline{\mathbf{S}}(n,\, 2,\, R_1) = \left\{ \prod_{j=2}^{N-1} \underline{\underline{\mathbf{T}}}(n,\, j,\, R_{j-1})\underline{\underline{\mathbf{T}}}^{-1}(n,\, j,\, R_j) \right\} \underline{\mathbf{S}}(n,\, N,\, R_{N-1}) \tag{24}$$

which may be written as:

$$\underline{\mathbf{S}}(n,\, 2,\, R_1) = \underline{\underline{\mathbf{H}}}^{(n)}\ \underline{\mathbf{X}}_{n,N} \tag{25}$$

where $\underline{\underline{\mathbf{H}}}^{(n)}$ is a 6x6 complex matrix.

At the borehole wall the boundary conditions involve only u, σ_{rr}, $\sigma_{r\theta}$, and σ_{rz}, the last two being zero for the bore fluid. Taking into account the multipole point source, and denoting by the superscript * the "reduced" displacement-stress vectors (i.e., which only contains u, σ_{rr}, $\sigma_{r\theta}$, and σ_{rz}), the system to be solved can be written in a matrix form as:

$$\left\{ \begin{array}{rcl} \underline{\mathbf{S}}^*(n,\,1,\,R_1) + \underline{Y}^{(n)} & = & \underline{\mathbf{S}}^*(n,\,2,\,R_1) \\ & = & \underline{\underline{\mathbf{H}}}^{(n),*}\,\underline{\mathbf{X}}_{n,N} \end{array} \right. \tag{26}$$

i.e.,

$$\underline{\underline{M}}^{(n)}\,\underline{Y}^{(n)} = \underline{W}^{(n)} \tag{27}$$

where

$\underline{\underline{M}}^{(n)}$ is a 4x4 complex matrix,

$\underline{Y}^{(n)} = (-u(n,\,s,\,R_1),\,-\sigma_{rr}(n,\,s,\,R_1),0,\,0)^T$

$\underline{W}^{(n)} = (A_{n1},\,B_{nN},\,D_{nN},\,F_{nN})^T$

where $u(n,\,s,\,R_1)$ and $\sigma_{rr}(n,\,s,\,R_1)$ are the displacement and the stress radiated by the source at $r = R_1$, i.e.,:

$$\left\{ \begin{array}{rcl} u(n,\,s,\,R_1) & = & \dfrac{1}{n!}\left(\dfrac{kp_1\,R_0}{2}\right)^n \varepsilon_n \left\{ \dfrac{n}{R_1} K_n(kp_1\,R_1) - kp_1 K_{n+1}(kp_1\,R_1) \right\} e^{i(kz-\omega t)} \\ \sigma_{rr}(n,\,s,\,R_1) & = & -\varepsilon_n \rho_1 \omega^2 \dfrac{1}{n!}\left(\dfrac{kp_1\,R_0}{2}\right)^n K_n(kp_1\,R_1) e^{i(kz-\omega t)} \end{array} \right. \tag{28}$$

Full waveform synthetic microseismograms

As the formulation of Kurkjian and Chang (1986) has been followed, the analysis is limited to the study of the field on the axis of the borehole. It is then assumed that "pressure sensors are used if the source is a monopole, that displacement sensors are used if the source is a dipole, that the spatial derivative of displacement is sensed if the source is a quadrupole and that other gradients are sensed for a multipole source of higher order". One then obtains:

- if the source is a monopole:

$$P(z,\,t) = \int_{-\infty}^{+\infty} S(\omega) D^{(0)}(\omega) e^{-i\omega t} d\omega + \int_{-\infty}^{+\infty}\int_{-\infty}^{+\infty} A_{01} S(\omega) e^{ikz} e^{-i\omega t} dk d\omega \tag{29}$$

- if the source is a multipole of the n-th order:

$$Re^{(n)}(z,\,t) = \int_{-\infty}^{+\infty} S(\omega) D^{(n)}(\omega) e^{-i\omega t} d\omega + \frac{R_0^n}{2^{2n} n!} \int_{-\infty}^{+\infty} \int_{-\infty}^{+\infty} (kp_1)^{2n} A_{n1} S(\omega) e^{ikz} e^{-i\omega t} dk d\omega \tag{30}$$

where

$S(\omega)$ denotes the source spectrum,

$D^{(n)}(\omega)$ is the source contribution given by:

$$D^{(n)}(\omega) = \frac{\pi \varepsilon_n R_0^n}{n!\, 2^{2n}} \sum_{m=0}^{n} C_m^n \frac{2^m}{\alpha_1^m} (-i\omega)^m \frac{(2n-m)!}{z^{2n-m+1}} e^{i\frac{\omega}{\alpha_1} z}$$

where C_m^n is the binomial factor.

NUMERICAL EXAMPLES

In this section, we analyze the dispersion and attenuation of the modes generated by dipole and quadrupole sources in various configurations. We will essentially focus on the fundamental modes. For each configuration, the study is divided into two parts referring to the cases of a fast and slow virgin sandstone. The formation parameters are given in Table 1. The multipole separation is 1 cm, while the borehole radius is 10 cm, unless specified otherwise. In every dispersion figure, the phase and group velocities of the modes are normalized with respect to the bore fluid, which is water (see Table 1), velocity.

Also analyzed are synthetic microseismograms computed at 256 points in time, the source waveform being a nonzero phase Ricker wavelet. The indicated arrival times have been computed using ray theory. When impossible, the indicated times correspond to the offset divided by the wave velocity.

Simple hole model

Fast formation

In the presence of a fast formation, a usual monopole (axisymmetric) source excites two types of waves. They are the Stoneley wave and the pseudo-Rayleigh modes (Figure 1). The Stoneley wave has no cut-off frequency. Its phase velocity starts at zero frequency with the so-called tube wave velocity and increases with frequency toward that of a Scholte wave (i.e., the high frequency limit of a Stoneley wave on a planar fluid-solid interface). Its dispersion is then slightly reversed. Its attenuation is practically constant in the entire frequency range, close to that of the bore fluid. The pseudo-Rayleigh modes have a low cut-off frequency, which increases with each higher mode. Their phase (and group) velocity starts at the formation shear velocity and decreases with frequency toward the bore fluid velocity. As described by Paillet and White (1982), the high frequency limit corresponds to that of a normal mode in an equivalent plane layer configuration (with a phase shift of $\pi/4$.) Their attenuation starts at the formation shear wave attenuation and tends toward that of the bore fluid at higher frequencies. It exhibits a strong intermediate maximum, correlated with the Airy phase (i.e., the minimum group velocity) of the mode.

Similarly, the multipole sources excite two types of waves in such a configuration. The fundamental modes are the counterpart of Stoneley waves, while the other ones behave like the pseudo-Rayleigh modes.

Figure 2 shows the dispersion and attenuation curves of the fundamental (referred to as the flexural) mode and first mode excited by a dipole source. Also displayed are their excitation curves computed following the residue theory (Kurkjian, 1985; Burns, 1986).

The flexural mode, which is associated with a pure bending of the hole, has no theoretical cut-off frequency, similar to the empty borehole case (Borstrom and Burden, 1982) and as already stated by Kumar and Ran (1969), and Roever et al. (1974), and, in the case of a horizontal acoustic point force, by Kurkjian (1986). Its phase velocity ranges from the formation shear velocity at zero frequency toward that of a Scholte wave, exhibiting a sharp direct dispersion. The high frequency limit is identical to that of a Stoneley wave. The absence of low frequency continuity on the figure is due to a coalescence of the pole related to the mode and the shear branch point beyond a given frequency, leading to a low energy shear event. The excitation curve corroborates this observation as it sharply drops off on two sides of a peak associated with the Airy phase of the mode, giving in practice a sharp low cut-off frequency. In the remainder of this paper, we will speak of useful starting energy. At low frequencies, the attenuation of the mode is equal to the formation shear wave attenuation, also emphasizing the shear wave limit and combination. It then greatly increases to reach a maximum corresponding to the Airy phase before decreasing toward the bore fluid attenuation at high frequencies. The high frequency behavior is then similar to that of the Stoneley wave.

The higher modes do have a low cut-off frequency which increases with each higher mode. As pointed out by Roever et al. (1974), the cut-off frequency of the first mode is very close to that of the first pseudo-Rayleigh mode excited by a monopole source (see Figure 1). For higher modes, the discrepancy is greater. Comparison of Figures 2 and 1 clearly shows the similarity between the dispersion and attenuation of the two modes. The excitation of the first mode is also typical of that of a pseudo-Rayleigh mode.

Such mode behavior leads to an important source center frequency effect, as shown in Figure 3. The source center frequency varies from .5 kHz to 10.5 kHz by steps of 500 Hz from top to bottom, the offset being equal to 5 m. Each waveform is normalized with respect to its own maximum. At low frequencies, the waveforms are dominated by a shear event associated with very low energy. As the frequency increases, the peak amplitude first increases and then decreases (see the scaling factors at the upper left), in accordance with the maximum of the excitation curve of the flexural mode (see Figure 2). With higher source center frequencies, high frequency shear events occur related to the trapped modes. Their contribution increases with the source center frequency. Contrary to the Stoneley wave from an axisymmetric monopole source, the low frequency part of the fundamental mode begins to arrive at the formation shear wave velocity.

Figure 4 displays the synthetic waveforms as a function of the offset with a 1 kHz (a) and 6 kHz (b) source center frequency. Provided that the shear wavelength is greater

than 10 times the borehole radius and that the offset is at least on the order of the shear wavelength, the borehole effects are minimal (Kurkjian, 1986). In such conditions, the geometric spreading of the shear wave is known to be proportional to $1/z$, while it is proportional to $1/z^2$ for the P wave. With a 1 kHz source center frequency, the shear wavelength is here equal to 2.16 m. The offset ranging from 2.4 m to 5 m, there is still a small borehole effect. Taking into account the attenuation, the peak amplitude ratio should be equal to 0.46 instead of 0.496 for the 1.4 m and 5 m offsets. Such a discrepancy decreases when considering a larger initial offset such as 4 m.

Similar to the dipole source, the quadrupole source excites a fundamental mode (referred to as the screw mode) and higher order modes (Figure 5).

There have been controversial discussions on the existence of a low cut-off frequency for the screw mode. Avoiding additional arguments in one way or another, we will speak of useful starting energy. This is justified in the sense that the dispersion, attenuation, and excitation (Figure 5c) of the screw mode are analogous to those of the flexural mode (Figure 2) with a shift toward higher frequency. The useful starting energy begins more sharply, around 6 kHz instead of 2 kHz for the present example. The characteristics of the higher mode are also similar to those of the mode generated either by a dipole (Figure 2) or a monopole source (Figure 1) with again a shift toward higher frequency.

In the time domain, the geometric spreading of the body waves is now proportional to $1/z^3$ and $1/z^2$, respectively for the P and S waves. Figure 6a shows the low frequency shear event obtained with a 1.5 kHz source center frequency. Due to the shift to higher frequencies, the Airy phase of the mode will occur with a higher source center frequency than with the dipole (Figure 6b). As for the dipole source, the first large amplitude arrival travels at the formation shear velocity, whatever the source center frequency.

Figure 8 shows the dispersion and attenuation curves of the flexural (a) and screw mode (b) in the presence of granite (1), limestone (2), and sandstone (3) (see Table 1). In both cases, as the formation shear velocity increases, the direct dispersion is more pronounced because the high frequency limit only varies a little. Correlatively, the maximum of attenuation increases while the useful starting energy is slightly shifted toward higher frequencies. The fundamental modes generated by multipole sources are then more sensitive to the formation rigidity than the Stoneley wave in the low frequencies. The borehole radius has little effect. When decreasing, the useful starting energy, as well as the Airy phase of the modes, is shifted toward higher frequencies. The reverse phenomenon occurs when it increases. On the other hand, the corresponding attenuation maximum is not modified. To summarize, the variation of the dispersion and attenuation of the fundamental modes as a function of the borehole radius is just a function of the wavenumber times the borehole radius. Being similar to the Stoneley wave at high frequencies, the maximum of excitation of the mode will increase with decreasing borehole radius.

Slow formation

Similarly to the case of a monopole source, the multipole source only excites fundamental modes in the presence of a slow formation. Figure 8a shows the dispersion and attenuation of the Stoneley wave (0), the flexural mode (1) and the screw mode (2), when the surrounding formation is a slow sandstone (Table 1).

Stoneley wave phase velocity dispersion is now direct, starting at the tube wave velocity (here less than the formation shear wave velocity) at zero frequency and tending toward that of Scholte wave at higher frequencies. Its attenuation decreases with frequency as compared to the fast formation case, the Stoneley wave is more coupled to the formation.

The phase (and group) velocity of both flexural and screw modes starts at the formation shear wave velocity and tends toward that of a Sholte wave at higher frequencies. The direct dispersion is then slightly more pronounced than for the Stoneley wave, as the high frequency limits are identical. Their low frequency attenuation follows that of the shear wave of the formation. Compared to the fast formation, their useful starting energy is located lower in frequency. Figure 8b displays the dispersion and attenuation of the flexural mode when the shear wave velocity of the slow sandstone (2) is decreased by 10 % (1) and increased by 10 % (3). This calculation demonstrates the sensitivity to the formation S-wave velocity and attenuation at low frequencies, and the decrease of the coupling of the mode with the formation as the rigidity increases. Such a trend is emphasized by the increase of the attenuation of the mode at high frequencies as it is more influenced by the bore fluid attenuation.

The excitation of the fundamental modes is similar to that in the presence of the fast formation (Figures 2c and 3c, respectively). They exhibit a maximum correlated with the Airy phase of the mode, and drop off on two sides of the peak. Such a behavior is illustrated in Figure 9 with a dipole source. For an offset of 4 m, the source center frequency varies from .5 kHz to 10.5 kHz from the top to the bottom. The maximum peak amplitude of the whole series occurs at 4 kHz and decreases for values above and below, more sharply in the latter case. At high frequencies, the P wavetrain dominates the waveform. As in the axisymmetric case configuration (Cheng and Toksöz, 1981), its absolute amplitude will decrease with decreasing Poisson's ratio. Similar results are obtained with the quadrupole source, although the significant amplitude of the P wave occurs higher in frequency.

For the present example, the shear wavelength is now equal to 1.2 m with a 1 kHz source center frequency. The required conditions being unfulfilled, the axial decay of the low frequency shear event generated by a dipole source (Figure 10a) is seen to be less than $1/z$ (.54 instead of .42, including the attenuation factor). With a 3 kHz source

center frequency (Figure 10b), the flexural mode dominates the waveforms, while the P-wave begins to be detectable at the shortest offsets. The results obtained with a quadrupole source are displayed in Figures 11a, b, the source center frequency being respectively equal to 1 kHz and 6 kHz. The latter case shows the weakness of the P-wave excitation compared to the dipole source. Whatever the source center frequency and the order of the multipole, the low frequency part of the fundamental modes is seen to travel at the formation shear wave velocity.

Invaded zone

The formation can be altered in the vicinity of the borehole wall. We hereafter consider the case of an invaded zone, i.e., the presence of an intermediate layer whose velocities are less than the virgin formation velocities. In such a configuration, the inner borehole radius remains constant, the initial formation moving away from the borehole by an amount equal to the invaded zone thickness. In the following, we consider 8 cm and 16 cm for the latter parameter.

Fast formation

The invaded zone is modeled by decreasing both P- and S-wave velocities of the sandstone by 10%. The quality factors are also lowered (see Table 1). Figures 12a, b show the dispersion and attenuation of the flexural and screw mode, respectively. Cases (1) and (2) refer to the invaded zone thickness of 16 cm and 8 cm, while (3) and (4) correspond to the infinite virgin formation and invaded zone situations. Despite a greater shear wave attenuation and identical Poisson's ratios, the maxima of attenuation of the Airy phase of both fundamental modes are seen to be lower than in the presence of the semi-infinite invaded zone. This corresponds to the only decrease of the shear wave velocity and, hence, rigidity of the borehole wall.

Whatever the order of the source, the low frequency part of the modes starts with the virgin formation shear wave characteristics (velocity and attenuation). The useful starting energy is shifted toward lower frequencies with increasing invaded zone thickness. Higher in frequency, the properties of the modes tend toward those of the mode generated in the presence of the only invaded zone. The convergence phenomenon is more pronounced for the screw mode as the excitation is located higher in frequency. It leads to a greater sensitivity of the Airy phase of the mode to the invaded zone properties than for the dipole.

Displayed on Figure 13 are iso-offset (z = 5m) comparisons of the waveforms obtained in the presence of the only virgin formation (1) and the 8cm (2) and 16 cm (3)

thick invaded zone. The dotted lines indicate the arrival time of the invaded zone S wave, which is later than that of the virgin formation. With a 1 kHz source center frequency (Figure 13a), the low frequency shear event contain more energy with a thicker invaded zone. It is related to the shift toward lower frequencies of the useful starting energy. As a consequence, the axial attenuation is also slightly less pronounced due to more important apparent borehole effects. At intermediate frequencies (3 kHz, Figure 13b), the waveforms are close to one another both in shape and amplitude. With higher source center frequencies (6 kHz and 7.5 kHz, Figure 13c, d, respectively), the peak amplitude still varies little from one case to another but the internal dynamics are modified. With increasing thickness of the invaded zone, the absolute and relative amplitude of the P wavetrain increases as well as that of the high frequency events arriving close to the formation shear waves. Similarly to the axisymmetric case, the former phenomenon is related to a curvature, without rupture, of the P wavefronts so that the energy is focused. The latter one is related to the higher modes behavior. Similar to the pseudo-Rayleigh modes excited by a monopole, their cut-off frequency is shifted toward lower frequencies with increasing invaded zone thickness. For a given source center frequency, more of their energy is then taken into account. The presence of the more attenuating invaded zone is emphasized through a lower frequency content of the high velocity part of the wave packets.

Figures 14a-d show the result obtained with a quadrupole source. Due to a higher frequency location of the useful starting energy of the screw mode, the variations of the peak amplitude as a function of the invaded zone thickness are more pronounced with low source center frequencies than previously (Figure 14a, b relative to 1.5 kHz and 3 kHz). At higher frequencies (Figure 14c, d), only the higher modes energy is clearly detectable, as well as the increase of the group velocity of the Airy phase.

Slow formation

The invaded zone is now modeled by decreasing the P- and S-wave velocities of the formation by 15% and 10%, and the associated quality factors from 50 to 40 and 35, respectively. The Poisson's ratio of the invaded zone is then less than that of the virgin formation, increasing the effects of the former.

Figure 15 shows the dispersion and attenuation of the flexural (a) and screw (b) modes. Cases (1) and (4) now refer to the semi-infinite virgin and invaded formations, while (2) and (3) correspond to the presence of an 8 cm and 16 cm thick invaded zone. As in the presence of the fast formation, the phase velocity starts at the virgin formation shear wave velocity with a useful starting energy shifted toward lower frequencies with increasing thickness of the invaded zone. The strong coupling with the surrounding media leads to modifications of the Airy phase characteristics. For both multipole sources, it is lower compared to the presence of the only virgin formation or invaded

zone. It is shifted toward lower frequencies with a 16 cm thick invaded zone and toward higher frequencies with an 8 cm thick one. With the quadrupole source, the associated velocity is lower in the latter case while it is the reverse situation for the dipole source. The excitation curves also follow these variations in the frequency location. Higher in frequency, the modes related to the multilayered configuration are indistinguishable from that of the only invaded zone. The attenuation of the mode starts at the virgin formation wave attenuation. It then strongly increases, more rapidly with a thicker invaded zone, emphasizing the coupling with the intermediate layer.

The iso-offset (z = 5 m) comparisons of the wavetrains obtained with the dipole and the quadrupole source are displayed in Figure 16a-d and 17a-d, respectively. When the invaded zone is present (cases (2) = 8 cm, and (3) = 16cm), the arrows indicate the arrival time of its own shear wave. It is clearly seen that, whatever the source center frequency and the order of the multipole, the low frequency parts of the modes begins to arrive at the formation shear velocity. The repartition of the peak amplitudes for a given source center frequency (1 kHz (a), 3 kHz (b), 6 kHz (c), and 7.5 kHz (c)) is representative of the shift toward lower frequencies of the useful starting energy (1 kHz), the location in frequency of the maximum of excitation (correlated with the Airy phase), and the variation of attenuations as previously discussed. Also clearly detectable are the variations of the group velocity of the Airy phase. Compared to the fast formation example, the increase of the absolute and relative amplitude of the P wavetrain with the thickness of the invaded zone is more noticeable. This is especially true with the quadrupole source (Figure 17c, d), leading to a strong modification of the internal dynamics.

Such variations are illustrated as a function of the offset (from 2.4 m to 5 m, by steps of .2 m) for the dipole source with a 3 kHz source center frequency in Figures 18, and for the quadrupole source with a 6 kHz source center frequency in Figures 19. Cases (a) and (b) refer to the presence of a 8 cm and 16 cm thick invaded zone, respectively. The velocity contrast and thicknesses being small, the first P-wave arrival always belongs to the virgin formation (calculations performed with ray theory predict a cross-over between the two P waves around 1.4 m). The presence of the invaded zone is then barely detectable although the axial behavior of the wavetrains is strongly modified (Compare with Figure 10b and 11b, respectively for the dipole and quadrupole source).

Increasing the thickness and/or the velocity contrast, the presence of the intermediate layer will be more easily detectable through the first P- and S-wave arrivals as a function of the offset. On the other hand, the Airy phase of the fundamental modes will be more strongly affected by (and representative of) the inner layer, similar to the Stoneley wave in the axisymmetric configuration, whatever the formation (fast or slow).

Well-bonded cased hole

In the well-bonded cased hole configuration, the inner borehole radius is decreased by the amount of the casing and cement thickness. The physical properties of these last are given in Table 1. We analyze the effects of the thickness of the cement (cement 1 being the reference) as well as of its physical properties (cement 2). The thickness of the steel layer is held constant, equal to 1.02 cm. The original borehole radius is 10 cm.

Fast formation

The dispersion and attenuation of the flexural mode in the presence of the fast sandstone are displayed in Figure 20a. Case (1) refers to the open hole geometry while cases (2) and (3) correspond to the cased-hole situation with 1 cm and 3 cm thick cement, respectively. In the low frequencies, the mode still follows the formation shear wave characteristics. The useful starting energy is now shifted toward higher frequencies with decreasing borehole radius. At intermediate frequencies, the cement plays a dominant role leading to slightly lower Airy phase velocity with increasing thickness. The direct dispersion is stretched along a wider frequency range and is less sharp.The maximum of attenuation is also decreased, emphasizing the correlated decrease of rigidity.

For a given thickness (3 cm, Figure 20b), decreasing the shear velocity of the cement (cement 2, see Table 1), leads also to a decrease of the apparent rigidity (case (2)). As a result, the useful starting energy is slightly shifted toward lower frequency compared to the previous example (case (3)), as for the open hole geometry (see Figure 7a), while the maximum of attenuation is little reduced.

The behavior of the screw mode is again analogous (Figure 21a, b) although the cement effects occur closer to its useful energy due to the higher frequencies involved.

Figure 22a shows the waveforms obtained with the dipole source and a 1 kHz source center frequency in the presence of the 3 cm thick cement. Due to the shift toward higher frequencies of the useful starting energy, the low frequency shear event now contains less energy and it is slightly more attenuated compare to the open hole situation (Figure 4a). With a 6 kHz source center frequency (Figure 22b), the axial attenuation is again more pronounced (see Figure 4b) due to less high frequency events. This is related to the higher modes behavior which is similar to that of the pseudo-Rayleigh modes excited by a monopole. Their cut-off frequency are shifted toward higher frequencies while their dispersion and attenuation characterisitics are representative of the combined effects of the steel, the cement, and the formation (see Tubman et al., 1984; Burns, 1986). The waveforms obtained in the same configuration with the quadrupole source and a 6 kHz center frequency are displayed in Figure 23. The axial attenuation is less than

in the open hole configuration (Figure 6b) in accordance with the attenuation curves and because the higher modes play practically no role in any configuration (their cut-off frequency is too high).

Slow formation

In the axisymmetric configuration, the Stoneley wave is a leaky wave at low and high frequencies when logging in a well-bonded cased hole surrounded by a slow formation. Its phase velocity is greater than the formation shear wave velocity. Its excitation and attenuation properties emphasize the controlling effect of the casing and practically no sensitivity to the cement characteristics (Schoenberg et al., 1981; Schmitt and Bouchon, 1985; Tubman et al., 1984; Burns, 1986). The high frequency part of the fundamental modes excited either by a dipole or a quadrupole source will then also be leaky. This phenomenon will also be reinforced by the shift toward higher frequencies of the useful starting energy. As a result, it is only with a low source center frequency that the multipole tool will be capable of logging the slow formation shear wave velocity behind casing.

Such behavior is illustrated in the case of a dipole source in Figure 24. The thickness of the cement is 3 cm (cement 1, Table 1) while the formation is the slow sandstone. With a 1 kHz source center frequency (Figure 24a), the waveforms are composed of the dominant shear event related to the slow formation. Compared to the open hole situation (Figure 10a), the axial attenuation is much more pronounced. With a 3 kHz source center frequency (Figure 24b), the first noticeable arrival is now the P wave of the formation followed by high frequency events related to the cement layer. The flexural mode is seen to travel with a velocity higher than that of the formation shear wave (see Figure 10b). Increasing again the source center frequency (6 kHz, Figure 24c), the waveforms bear little resemblance to any of those previously obtained. Only the P wave of the formation is propagative. The low velocity events are totally leaky. Figure 25 show the waveforms obtained with a 1 kHz (a) and a 3 kHz (b) source center frequency when no cement is present. The similarity with those just analyzed emphasizes the controlling role of the casing layer as in the axisymmetric configuration. With a quadrupole source, these effects are even more critical because of the higher frequency location of the useful starting energy of the screw mode.

CONCLUSIONS

We have presented a general formulation based on the Thomson-Haskell method which allows the analysis of the wavefields generated by multipole sources in the presence

of a multilayered elastic formation. The results obtained from the different models investigated are summarized as follows.

A. Whatever the formation (fast or slow) and the configuration, the low frequency part of the fundamental modes follows the properties of the virgin formation shear wave. Their excitation sharply drops off on two sides of a peak associated with the Airy phase. Their high frequency part behaves like the Stoneley wave excited by a monopole source. For a given situation, the flexural mode excited by the dipole source exhibits useful starting energy lower in frequency than the screw mode excited by a quadrupole source.

B. The higher modes generated only when the surrounding formation is fast present characteristics similar to the pseudo-Rayleigh modes excited by monopole sources (dispersion, attenuation and excitation).

C. In the presence of an invaded zone, the useful starting energies of the fundamental modes are shifted toward lower frequencies with increasing thickness of the intermadiate layer, leading to more energy in the low frequency shear event which belongs to the virgin formation. Their intermediate and high frequency parts are strongly influenced by the inner layer properties. Such behavior increases with large velocity contrasts and/or thickness of the inner layer as well as with the order of the source. On the other hand, small velocity contrasts can modify the internal dynamics of the waveforms more easily in slow formations, through an increase of the P wavetrain. Whatever the formation properties and the source center frequency, the low frequency (high velocity) part of the guided wavetrain begins to arrive at the virgin formation velocity for sufficiently large offsets.

D. When the bore hole is cased and well bonded, the useful (low frequency) starting energy of the modes is shifted toward higher frequencies, due to the decrease in borehole radius. It still follows the formation shear wave characteristics. In the presence of a fast formation, the effects of the cement are predominant at intermediate frequencies.

E. When the cased hole is surrounded by a slow formation, it is only with low source center frequencies that multipole sources can log the formation shear wave due to the leaky character of the fundamental modes. The casing is the controlling layer.

ACKNOWLEDGEMENTS

This work was supported by the Full Waveform Acoustic Logging Consortium at M.I.T.

REFERENCES

Abramowitz, M., and Stegun, I.A., 1965, Handbook of Mathematical Functions. Dover publications.

Aki, K., and Richards, P.G., 1980, Quantitative Seismology. W.H. Freeman Co.

Baker, L.J., and Winbow, G.A., 1985, Multipole logging in invaded formations, Presented at the 55th Ann. Internat. Mtg. and Expos., Soc. Explor. Geophys., Washington.

Benzig, W.M., and Endres, A., 1983, Experimentation with down hole shear wave velocity measurements. Presented at the 53rd Ann. Internat. Mtg. and Expos., Soc. Explor. Geophys., Las Vegas.

Bostrom, A., and Burden, A., 1982, Propagation of elastic surface waves along a cylindrical cavity and their excitation by a point force, J. Acoust. Soc. Am., 72, 998-1004.

Burns, D.R., 1986, Formation property estimation from guided waves in a borehole, Ph.D. thesis, M.I.T., Cambridge.

Chen, S.T., 1984, Experimental studies of on-line shear wave logging. Presented at the 54th Ann. Internat. Mtg. and Expos., Soc. Explor. Geophys., Atlanta.

Chen, S.T., 1985, Shear wave logging with dipole sources, Presented at the 55th Ann. Internat. Mtg. and Expos., Soc. Explor. Geophys., Washington.

Cheng, C.H., and Toksöz, M.N., 1981, Elastic wave propagation in a fluid filled borehole and synthetic aoustic logs, Geophysics, 46, 1042-1053.

Everhart, A.H., and Chang, S.K., 1985, A theoretical study of dipole shear logging in cased holes, Presented at the 55th Ann. Internat. Mtg. and Expos., Soc. Explor. Geophys., Washington.

Gradshteyn, I.S., and Rhyzhik, I.M., 1965, Table of Integrals, Series and Products. Academic Press Inc.

Kitsunezaki, C., 1980, A new method for shear wave logging, Geophysics, 45, 489-1506.

Kurkjian, A.L., 1985, Numerical computation of individual far field arrivals excited by an acoustic source in a borehole, Geophysics, 50, 852-866.

Kurkjian, A.L., and Chang, S.K., 1986, Acoustic multipoles in fluid-filled boreholes, Geophysics, 51, 148-163.

Kurkjian, A.L., 1986, Theoretical far-field radiation from a low-frequency horizontal point force in a vertical borehole, Geophysics, 51, 930-939.

Roever, W., Rosenbaum, J., and Vining, T., 1974, Acoustic waves from an impulsive source in a fluid-filled borehole, J. Acoust. Soc. Am., 55, 1144-1157.

Schmitt, D.P., and Bouchon, M., 1985, Full wave acoustic logging: synthetic microseismograms and frequency wavenumber analysis, Geophysics, 50, 1756-1778.

Schoenberg, M., Marzetta, T., Aron, J., and Porter, R., 1981, Space time dependence of acoustic waves in a borehole , J. Acoust. Soc. Am., 70, 1496-1507.

Tongtaow, C., 1982, Wave propagation along a cylindrical borehole in a transversely isotropic medium. Ph.D. thesis, Colorado School of Mines.

Tubman, K.M., Cheng, C.H., and Toksöz, M.N., 1984, Synthetic full waveform acoustic logs in cased boreholes, Geophysics, 49, 1051-1059.

Watson, G.N., 1922, A Treatise on the Theory of Bessel Functions, Cambridge University Press.

White, J.E., 1967, The hula log - a proposed acoustic tool, Presented at the Soc. Prof. Well Log Analysts Conf.

Winbow, G., and Rice, J.A., 1984, Theoretical performance of multipole sonic logging tools, Presented at the 54th Ann. Internat. Mtg. and Expos., Soc. Explor. Geophys., Atlanta.

Winbow, G.A., 1985, Compressional and shear arrivals in a multiple sonic log, Geophysics, 50, 1119-1126.

Zemanek, J., Angona, F.A., Williams, D.M., and Caldwell, R.L., 1984, Continuous shear wave logging, Trans. SPWLA 25th Ann. Log. Symp., Paper U.

APPENDIX

Elements of the $\underline{\underline{\mathbf{T}}}(n, j, r)$ matrix

For simplicity the term $\frac{1}{n!}\left(\frac{kp_1 R_0}{2}\right)^n e^{ikz}e^{-i\omega t}$ as well the θ dependence are omitted. It has to be noted that the following formulae are the ones numerically used.

$$
\begin{aligned}
T_{11} &= \frac{n}{r}I_n(kp_j r) + kp_j I_{n+1}(kp_j r)\\
T_{12} &= \frac{n}{r}K_n(kp_j r) - kp_j K_{n+1}(kp_j r)\\
T_{13} &= \frac{n}{r}I_n(ks_j r)\\
T_{14} &= \frac{n}{r}K_n(ks_j r)\\
T_{15} &= ik\left\{\frac{n}{r}I_n(ks_j r) + ks_j I_{n+1}(ks_j r)\right\}\\
T_{16} &= ik\left\{\frac{n}{r}K_n(ks_j r) - ks_j K_{n+1}(ks_j r)\right\}
\end{aligned}
$$

$$
\begin{aligned}
T_{21} &= -\frac{n}{r}I_n(kp_j r)\\
T_{22} &= -\frac{n}{r}K_n(kp_j r)\\
T_{23} &= -\frac{n}{r}I_n(ks_j r) - ks_j I_{n+1}(ks_j r)\\
T_{24} &= -\frac{n}{r}K_n(ks_j r) + ks_j K_{n+1}(ks_j r)\\
T_{25} &= -\frac{ikn}{r}I_n(ks_j r)\\
T_{26} &= -\frac{ikn}{r}K_n(ks_j r)
\end{aligned}
$$

$$
\begin{aligned}
T_{31} &= ikI_n(kp_j r)\\
T_{32} &= ikK_n(kp_j r)\\
T_{33} &= 0\\
T_{34} &= 0\\
T_{35} &= -ks_j^2 I_n(ks_j r)\\
T_{36} &= -ks_j^2 K_n(ks_j r)
\end{aligned}
$$

$$
\begin{aligned}
T_{41} &= I_n(kp_j\,r)\left\{\rho_j\left[2\beta_j^2k^2-\omega^2\right]+2\frac{n(n-1)}{r^2}\rho_j\beta_j^2\right\}-\frac{2}{r}\rho_j\beta_j^2kp_jI_{n+1}(kp_j\,r)\\
T_{42} &= K_n(kp_j\,r)\left\{\rho_j\left[2\beta_j^2k^2-\omega^2\right]+2\frac{n(n-1)}{r^2}\rho_j\beta_j^2\right\}+\frac{2}{r}\rho_j\beta_j^2kp_jK_{n+1}(kp_j\,r)\\
T_{43} &= 2\rho_j\beta_j^2\left\{\frac{n(n-1)}{r^2}I_n(ks_j\,r)+\frac{n}{r}ks_jI_{n+1}(ks_j\,r)\right\}\\
T_{44} &= 2\rho_j\beta_j^2\left\{\frac{n(n-1)}{r^2}K_n(ks_j\,r)-\frac{n}{r}ks_jK_{n+1}(ks_j\,r)\right\}\\
T_{45} &= 2ik\rho_j\beta_j^2\left\{I_n(ks_j\,r)\left[\frac{n(n-1)}{r^2}+ks_j^2\right]-\frac{1}{r}ks_jI_{n+1}(ks_j\,r)\right\}\\
T_{46} &= 2ik\rho_j\beta_j^2\left\{K_n(ks_j\,r)\left[\frac{n(n-1)}{r^2}+ks_j^2\right]+\frac{1}{r}ks_jK_{n+1}(ks_j\,r)\right\}
\end{aligned}
$$

$$
\begin{aligned}
T_{51} &= -2\frac{n}{r}\rho_j\beta_j^2\left\{\frac{n-1}{r}I_n(kp_j\,r)+kp_jI_{n+1}(kp_j\,r)\right\}\\
T_{52} &= -2\frac{n}{r}\rho_j\beta_j^2\left\{\frac{n-1}{r}K_n(kp_j\,r)-kp_jK_{n+1}(kp_j\,r)\right\}\\
T_{53} &= \rho_j\beta_j^2\left\{I_n(ks_j\,r)\left[\frac{2n(1-n)}{r^2}-ks_j^2\right]+\frac{2}{r}ks_jI_{n+1}(ks_j\,r)\right\}\\
T_{54} &= \rho_j\beta_j^2\left\{K_n(ks_j\,r)\left[\frac{2n(1-n)}{r^2}-ks_j^2\right]-\frac{2}{r}ks_jK_{n+1}(ks_j\,r)\right\}\\
T_{55} &= 2\frac{ikn}{r}\rho_j\beta_j^2\left\{I_n(ks_j\,r)\frac{1-n}{r}-ks_jI_{n+1}(ks_j\,r)\right\}\\
T_{56} &= 2\frac{ikn}{r}\rho_j\beta_j^2\left\{K_n(ks_j\,r)\frac{1-n}{r}+ks_jK_{n+1}(ks_j\,r)\right\}
\end{aligned}
$$

$$
\begin{aligned}
T_{61} &= 2ik\rho_j\beta_j^2\left\{\frac{n}{r}I_n(kp_j\,r)+kp_jI_{n+1}(kp_j\,r)\right\}\\
T_{62} &= 2ik\rho_j\beta_j^2\left\{\frac{n}{r}K_n(kp_j\,r)-kp_jK_{n+1}(kp_j\,r)\right\}\\
T_{63} &= i\frac{kn}{r}\rho_j\beta_j^2I_n(ks_j\,r)\\
T_{64} &= i\frac{kn}{r}\rho_j\beta_j^2K_n(ks_j\,r)\\
T_{65} &= \left(\frac{\omega^2}{\beta_j^2}-2k^2\right)\rho_j\beta_j^2\left\{\frac{n}{r}I_n(ks_j\,r)+ks_jI_{n+1}(ks_j\,r)\right\}\\
T_{66} &= \left(\frac{\omega^2}{\beta_j^2}-2k^2\right)\rho_j\beta_j^2\left\{\frac{n}{r}K_n(ks_j\,r)-ks_jK_{n+1}(ks_j\,r)\right\}
\end{aligned}
$$

TABLE

Layer	α (m/s)	β (m/s)	ρ (kg/m^3)	Q_α	Q_β
Water	1500	0	1000	30	
Fast sandstone	4878	2601	2160	60	60
Invaded zone	4390	2341	2360	40	40
Limestone	5081	2771	2160	60	60
Granite	5881	3750	2160	60	60
Slow sandstone	2751	1201	2100	50	50
Invaded zone	2338	1081	2000	40	35
Casing	6098	3354	7500	1000	1000
Cement 1	2823	1729	1920	40	30
Cement 2	2823	1555	1730	40	30

Table 1. Layer parameters.

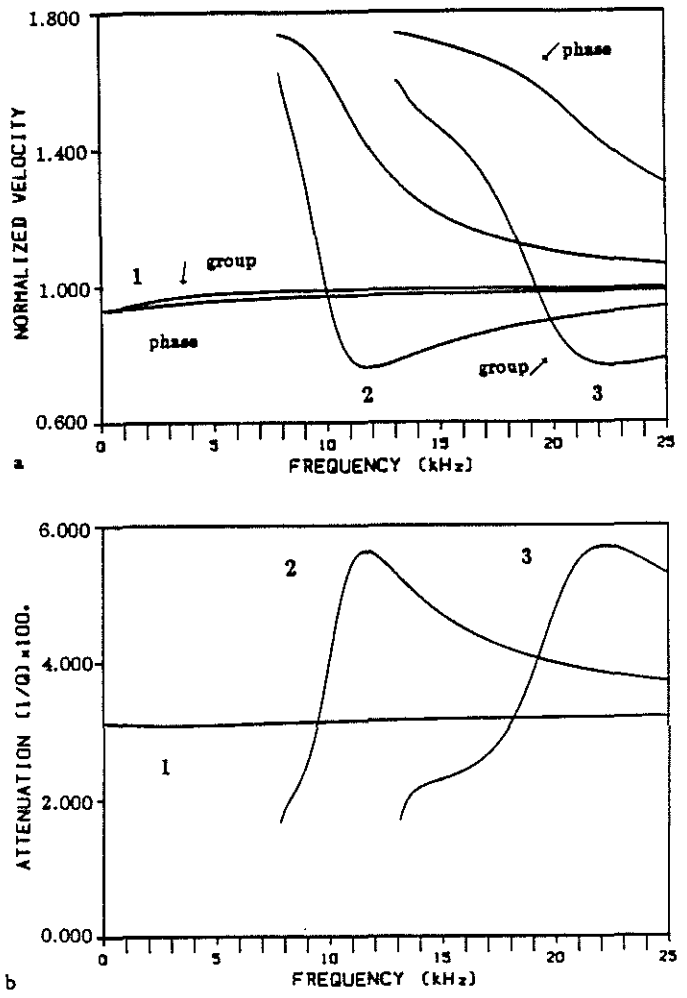

Figure 1: Monopole source. Dispersion (a) and attenuation (b) of the Stoneley wave (1) and the first two pseudo-Rayleigh modes ((2) and (3)) in the presence of a fast sandstone. The velocities are normalized with respect to the bore fluid velocity.

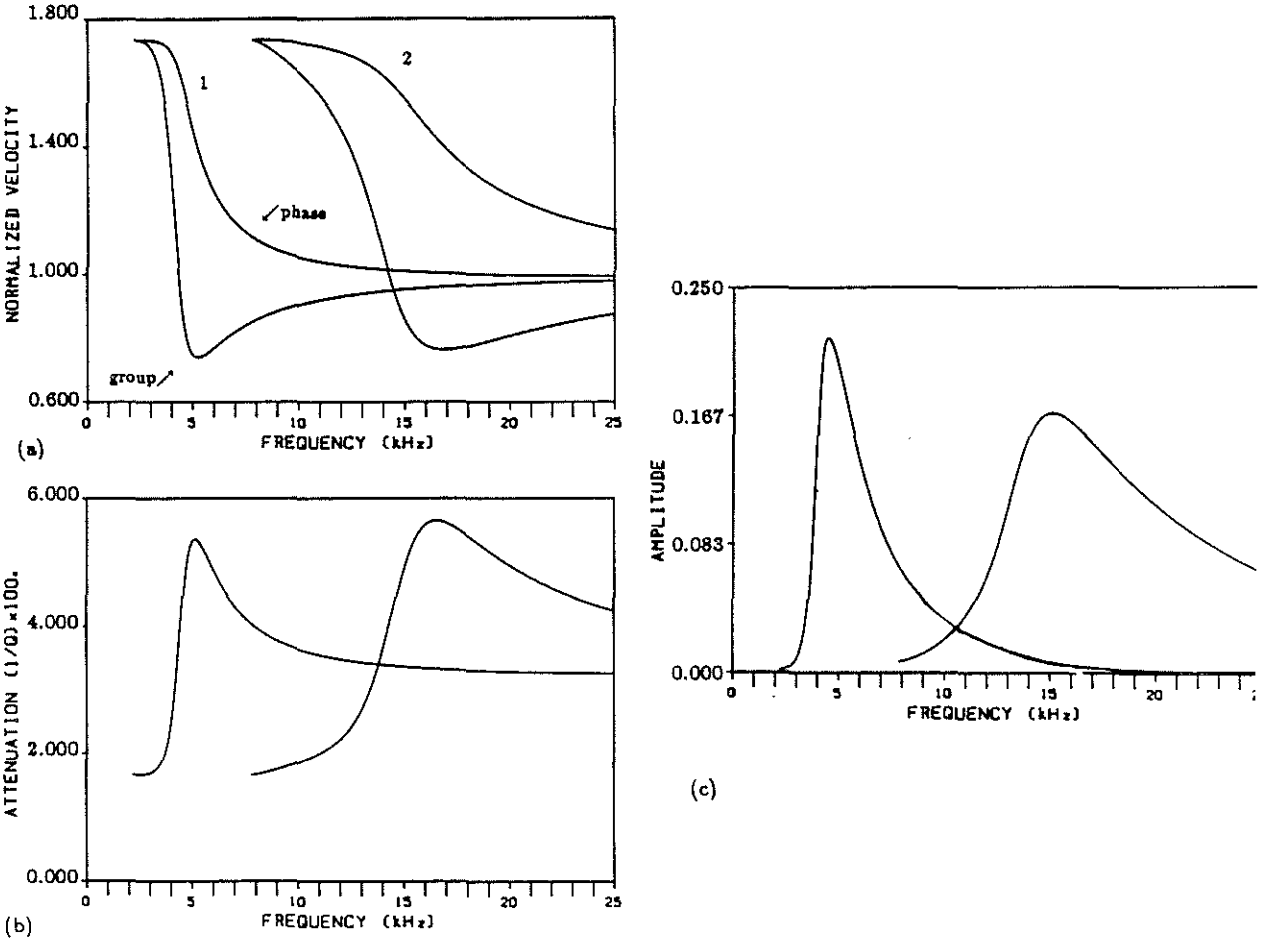

Figure 2: Dipole source. Dispersion (a), attenuation (b), and excitation (c) of the flexural mode (1) and the first trapped mode (2) in the presence of a fast sandstone. The velocities are normalized with respect to the bore fluid velocity.

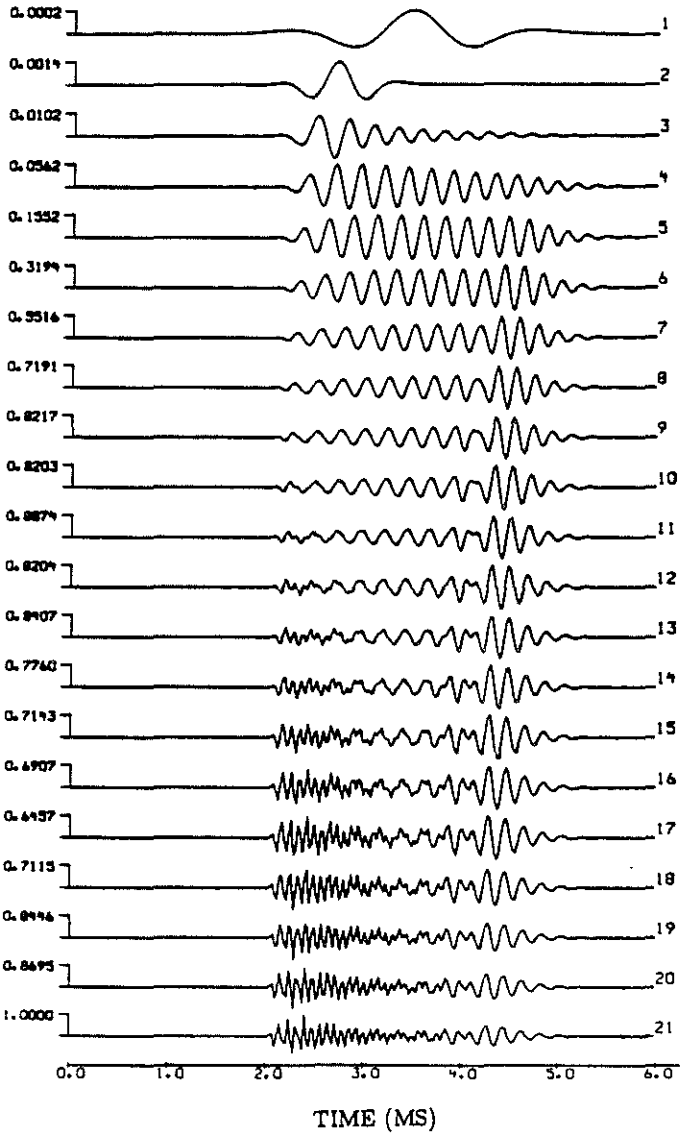

Figure 3: Dipole source, fast sandstone. Source center frequency effects. The offset is equal to 5 m. The source center frequency varies from .5 kHz to 10.5 kHz by steps of .5 kHz from the top to the bottom. Each waveform is normalized with respect to its own peak amplitude. The scaling factor at the upper left gives the relative value compared to the maximum of the whole series denoted by 1.00.

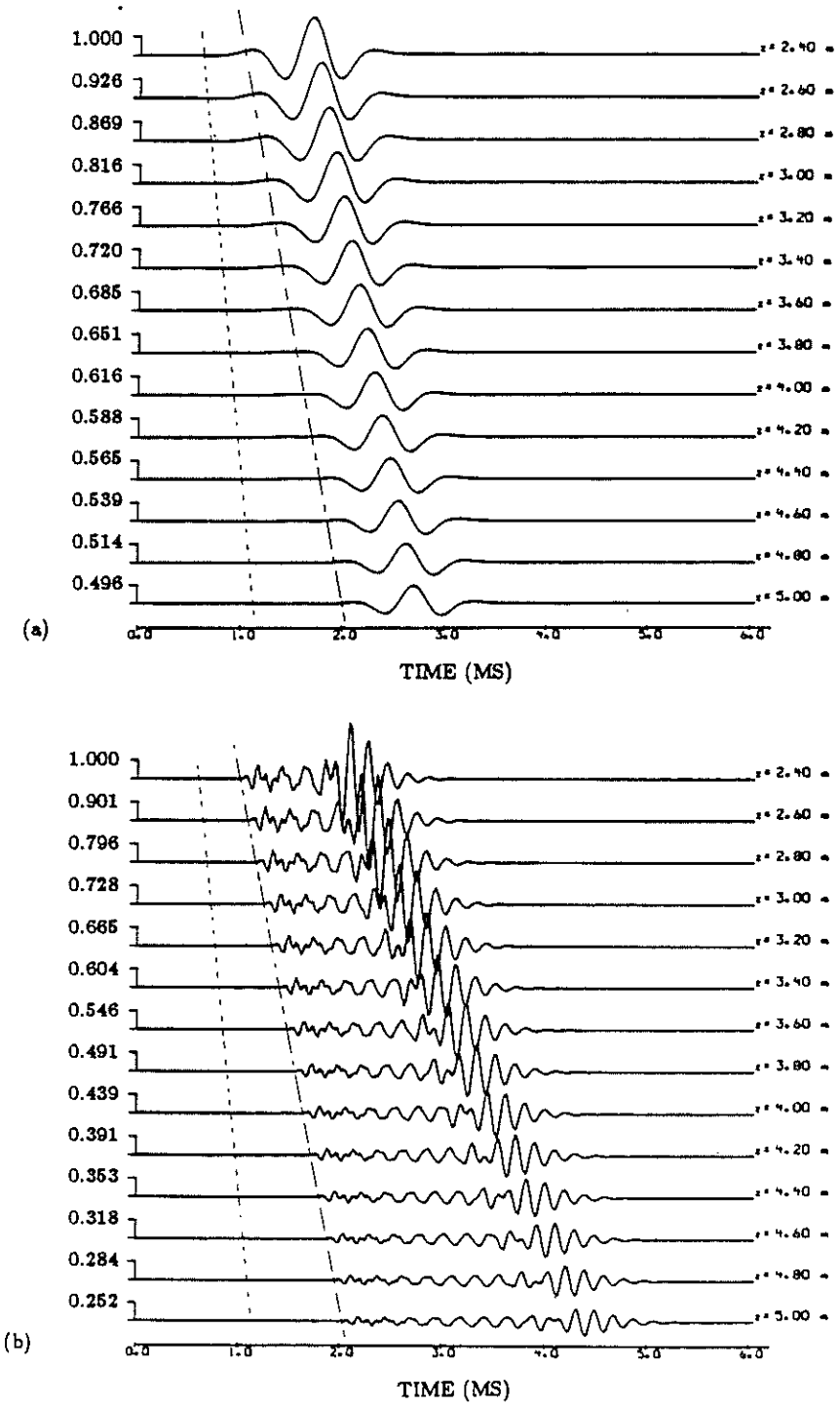

Figure 4: Dipole source, fast sandstone. Shot point obtained with a 1 kHz (a) and a 6 kHz (b) source center frequency. Each series is normalized with respect to its own maximum denoted by 1.00.

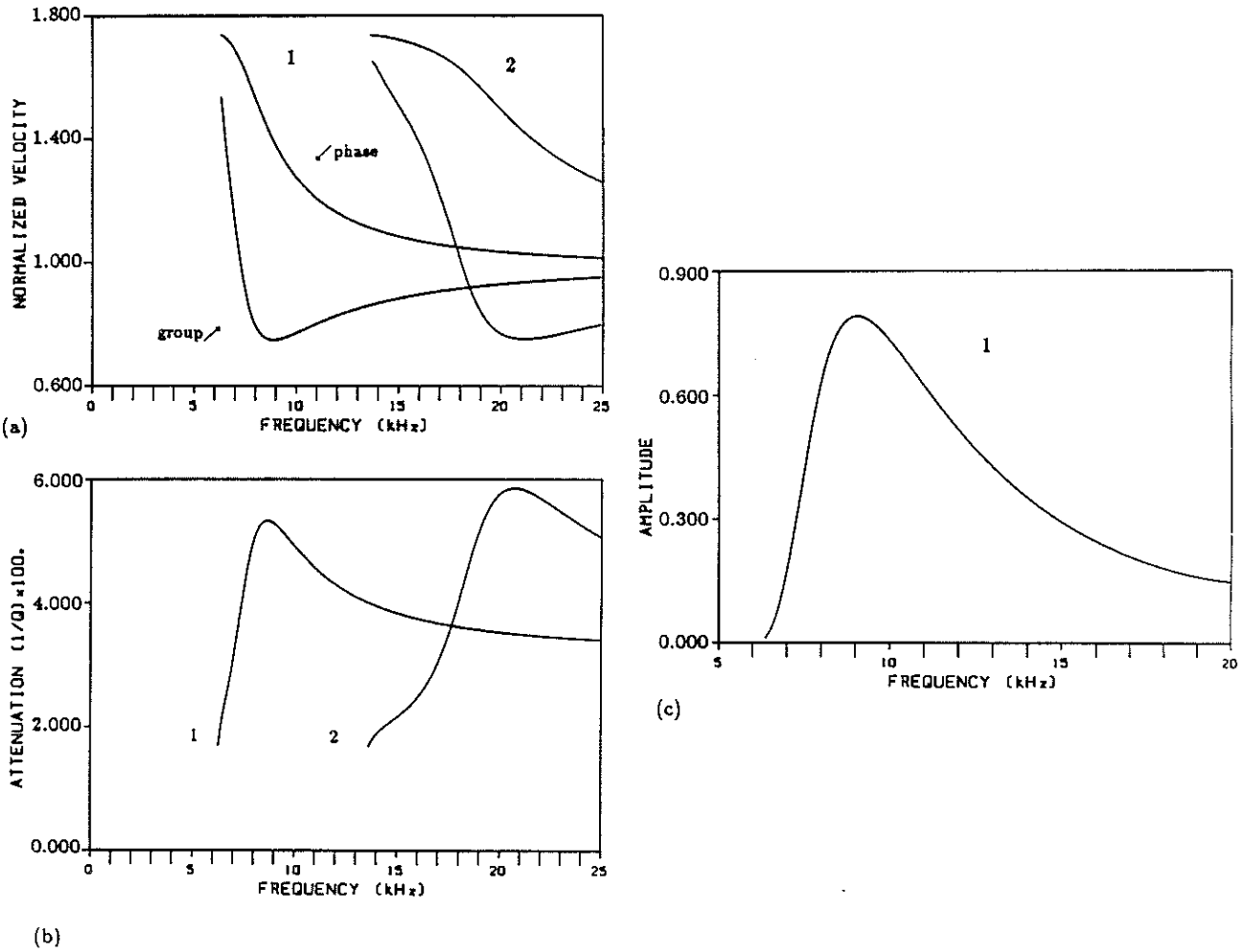

Figure 5: Quadrupole source. Dispersion (a), attenuation (b), and excitation (c) of the screw mode (1) and the first trapped mode (2) in the presence of a fast sandstone. The velocities are normalized with respect to the bore fluid velocity.

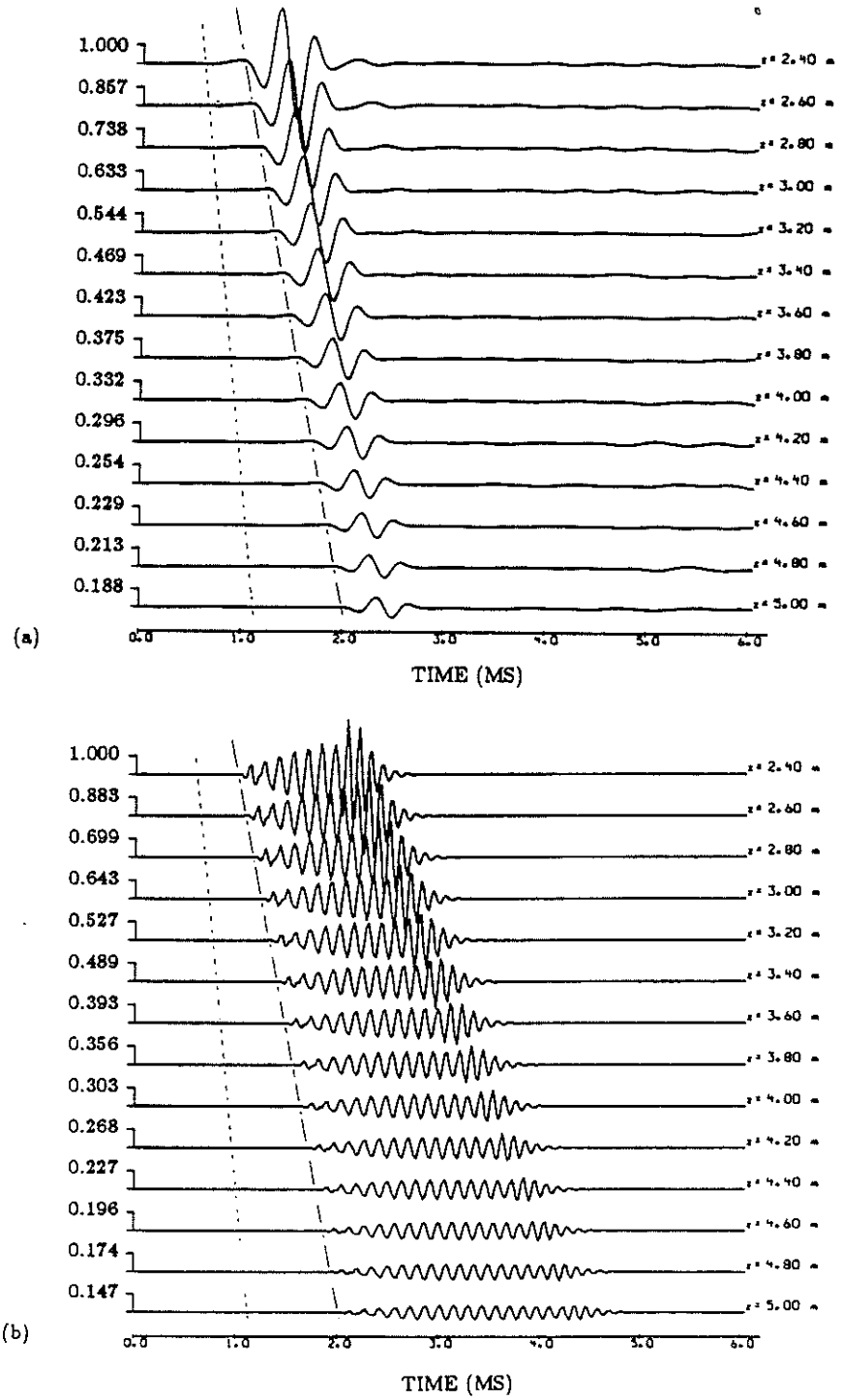

Figure 6: Quadrupole source, fast sandstone. Shot point obtained with a 1.5 kHz (a) and a 6 kHz (b) source center frequency. Each series is normalized with respect to its own maximum denoted by 1.00.

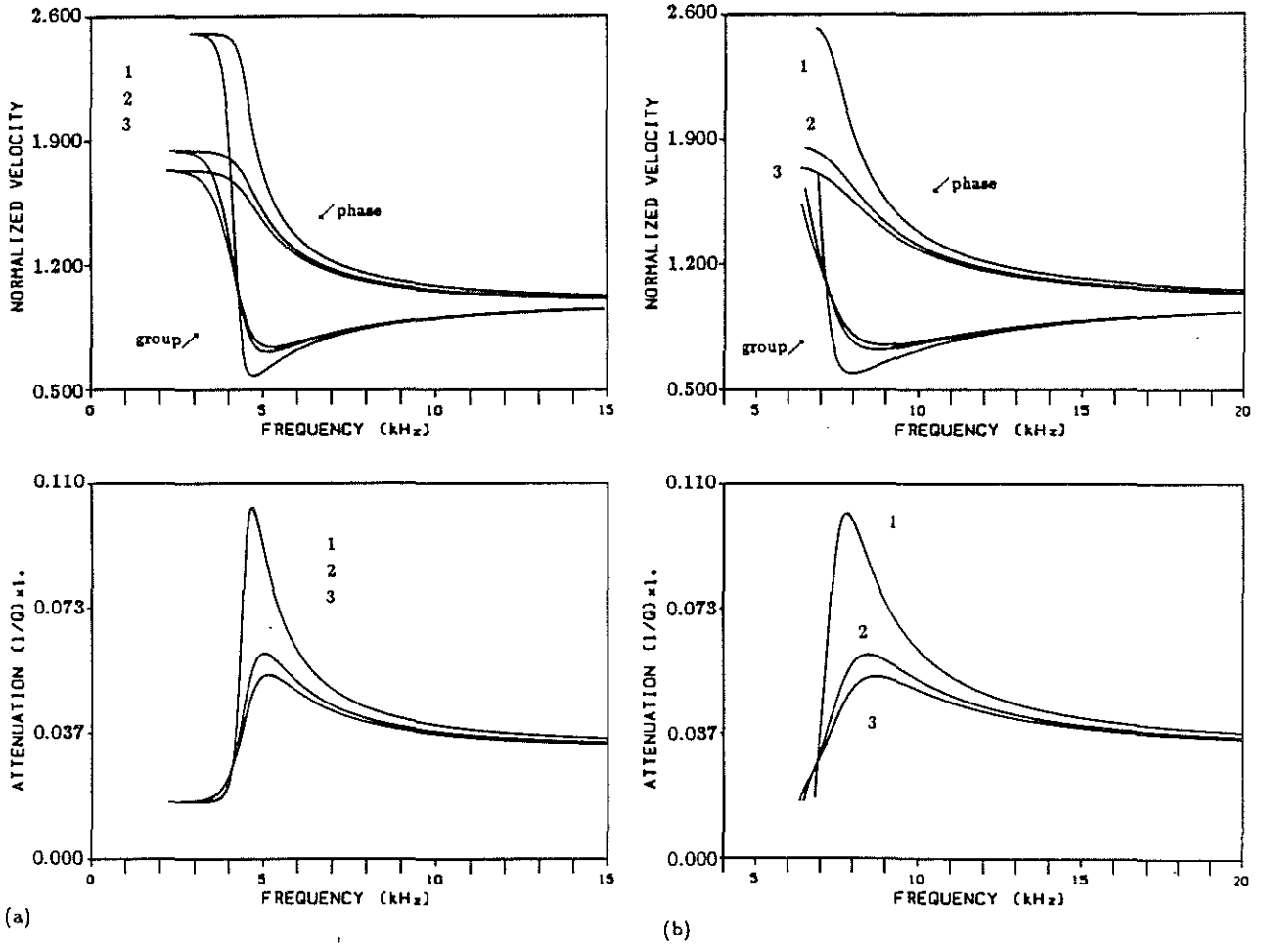

Figure 7: Dispersion and attenuation of the flexural (a) and screw (b) modes excited in the presence of granite (1), limestone (2), and a fast sandstone. The velocities are normalized with respect to the bore fluid velocity.

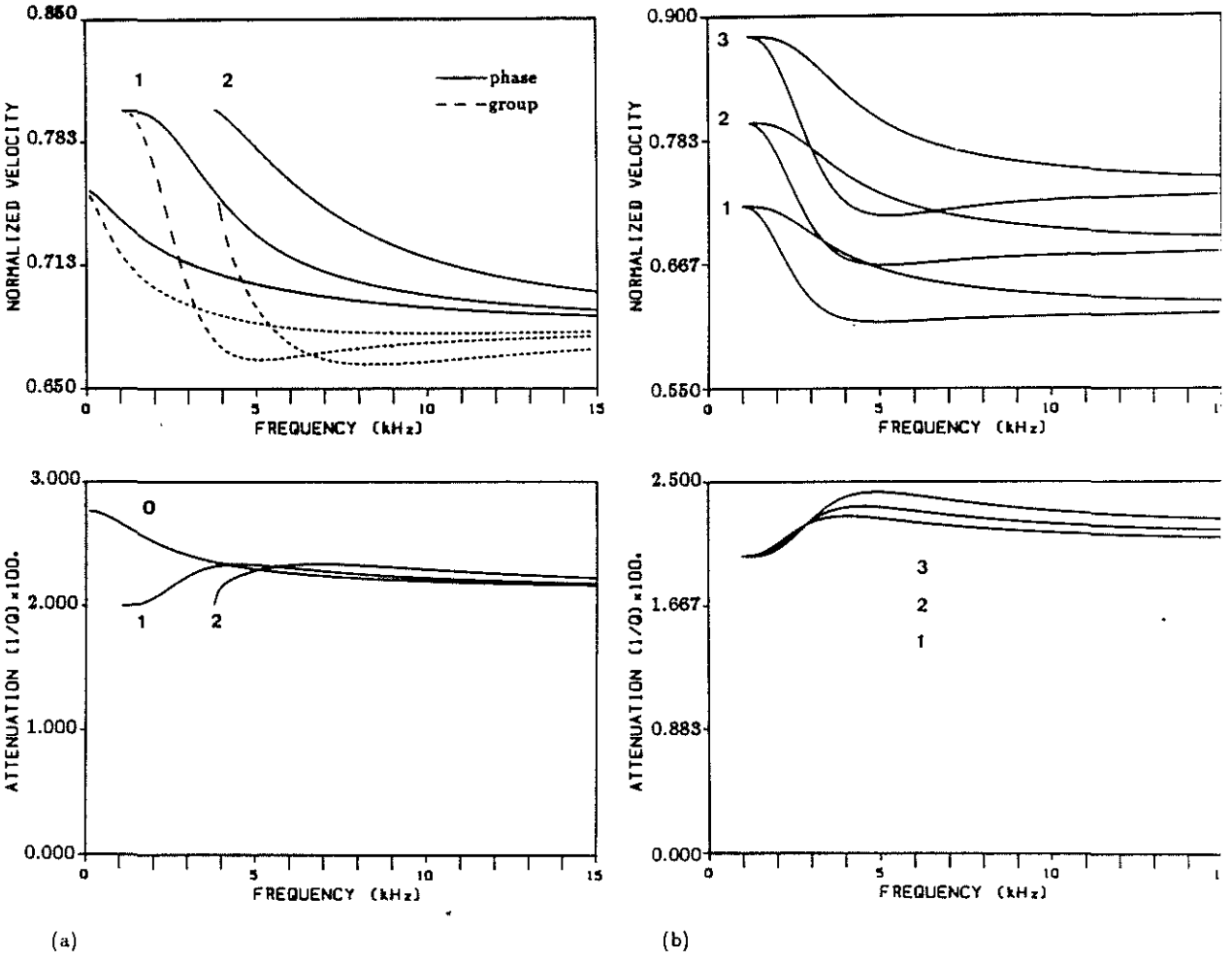

Figure 8: Slow sandstone. (a): Dispersion and attenuation of the Stoneley wave (0), the flexural and screw (2) modes excited by a monopole, dipole, and quadrupole source respectively. (b): Dispersion and attenuation of the flexural mode generated in the presence of a slow sandstone (2) and when the shear wave velocity is increased by 10% (2) and decreased by 10% (3). The velocities are normalized with respect to the bore fluid velocity.

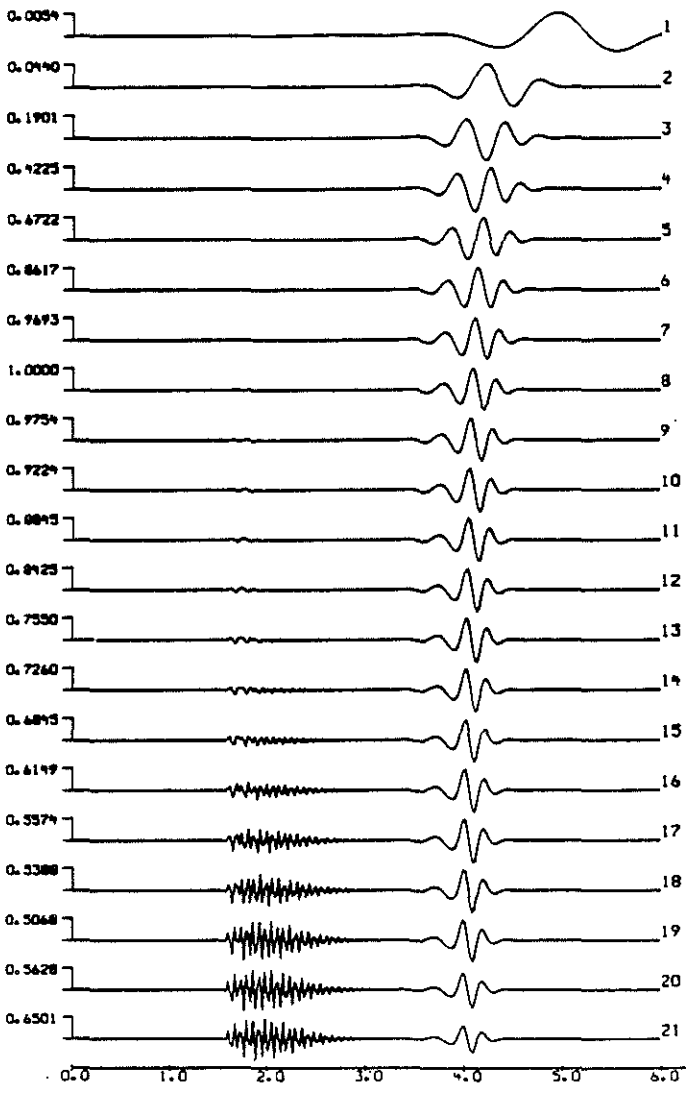

Figure 9: Dipole source, slow sandstone. Source center frequency effects. The offset is equal to 4 m. The source center frequency varies from .5 kHz to 10.5 kHz by steps of .5 kHz from the top to the bottom. Each waveform is normalized with respect to its own peak amplitude. The scaling factor at the upper left gives the relative value compared to the maximum of the whole series denoted by 1.00.

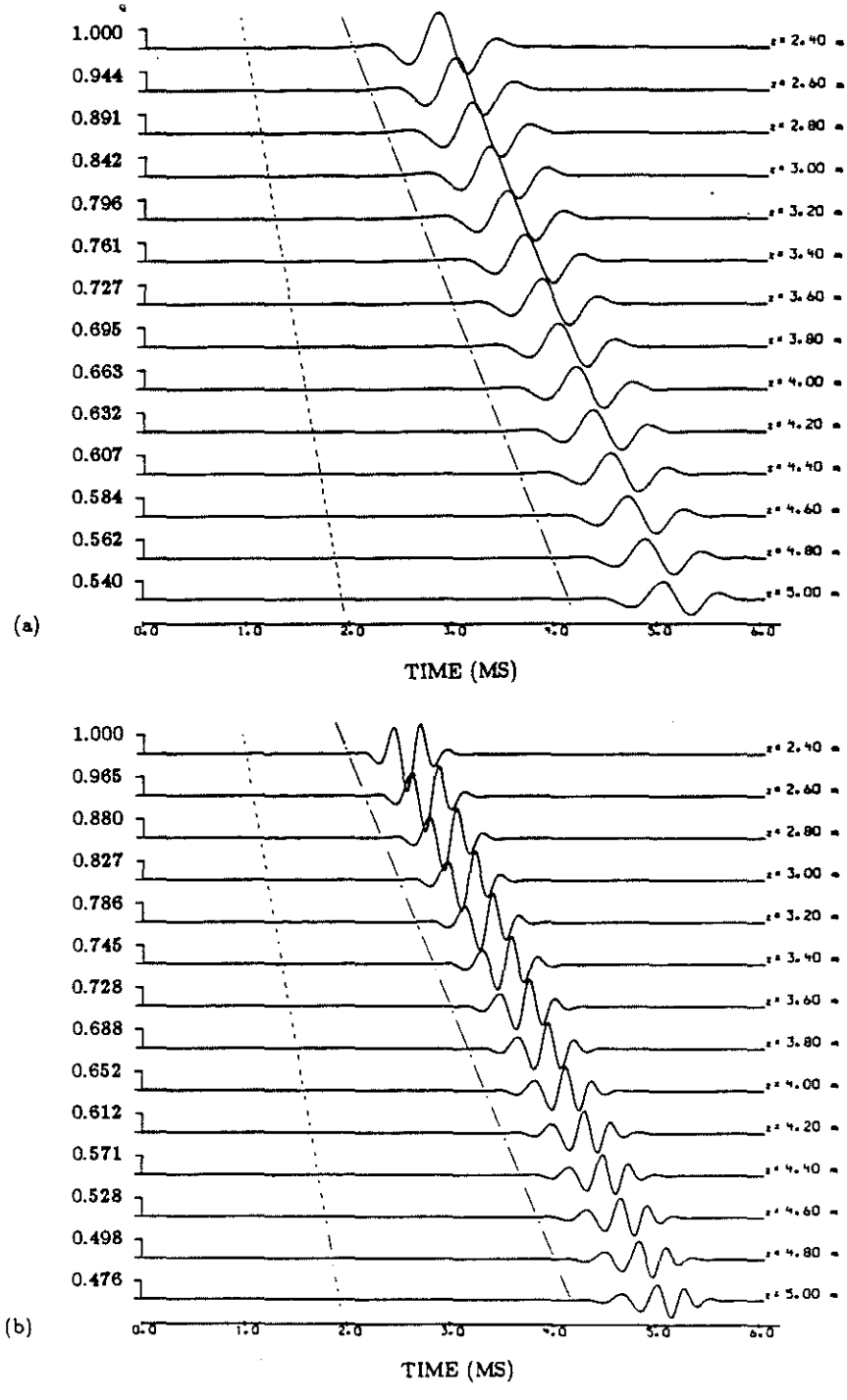

Figure 10: Dipole source, slow sandstone. Shot point obtained with a 1 kHz (a) and a 3 kHz (b) source center frequency. Each series is normalized with respect to its own maximum denoted by 1.00.

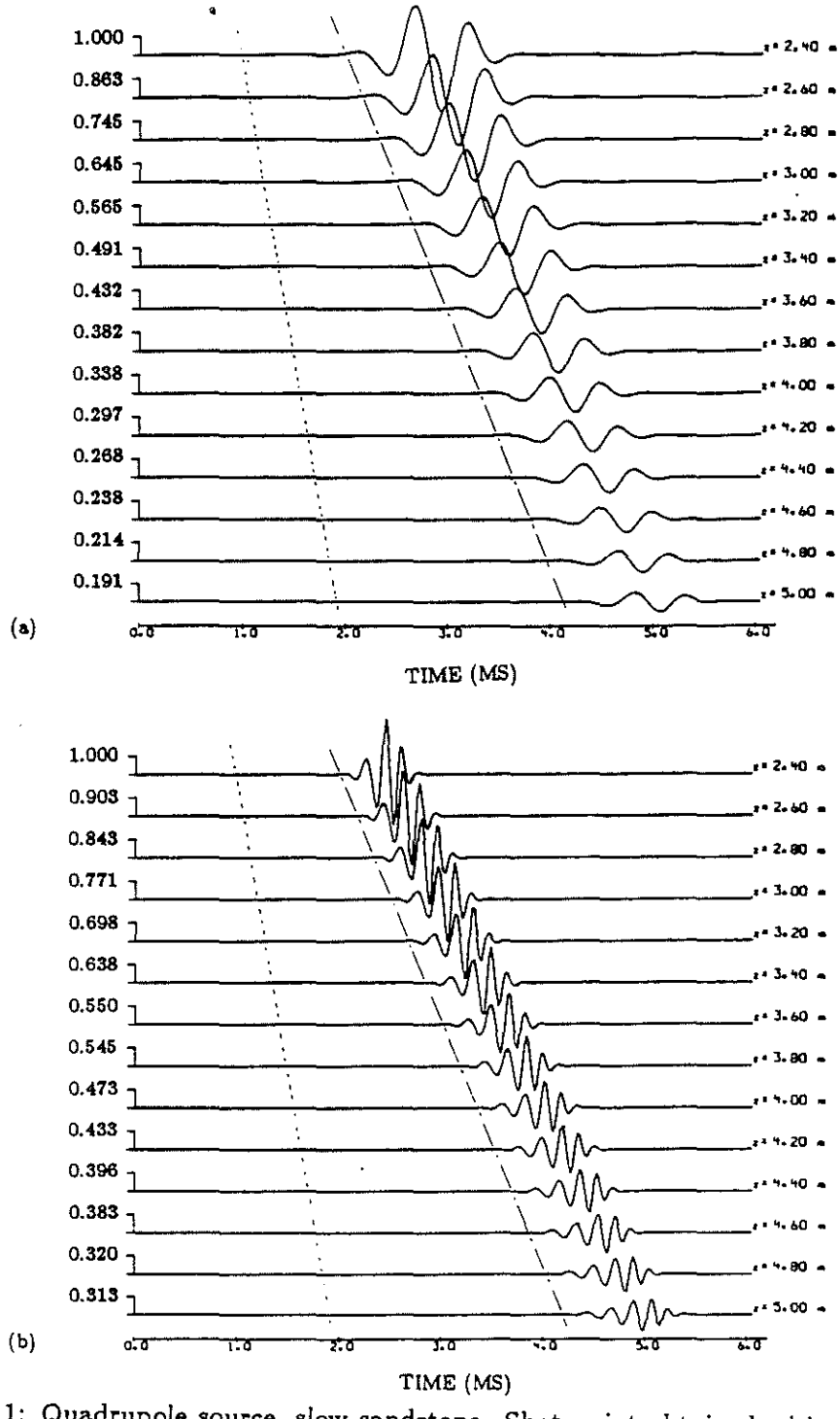

Figure 11: Quadrupole source, slow sandstone. Shot point obtained with a 1 kHz (a) and a 6 kHz (b) source center frequency. Each series is normalized with respect to its own maximum denoted by 1.00.

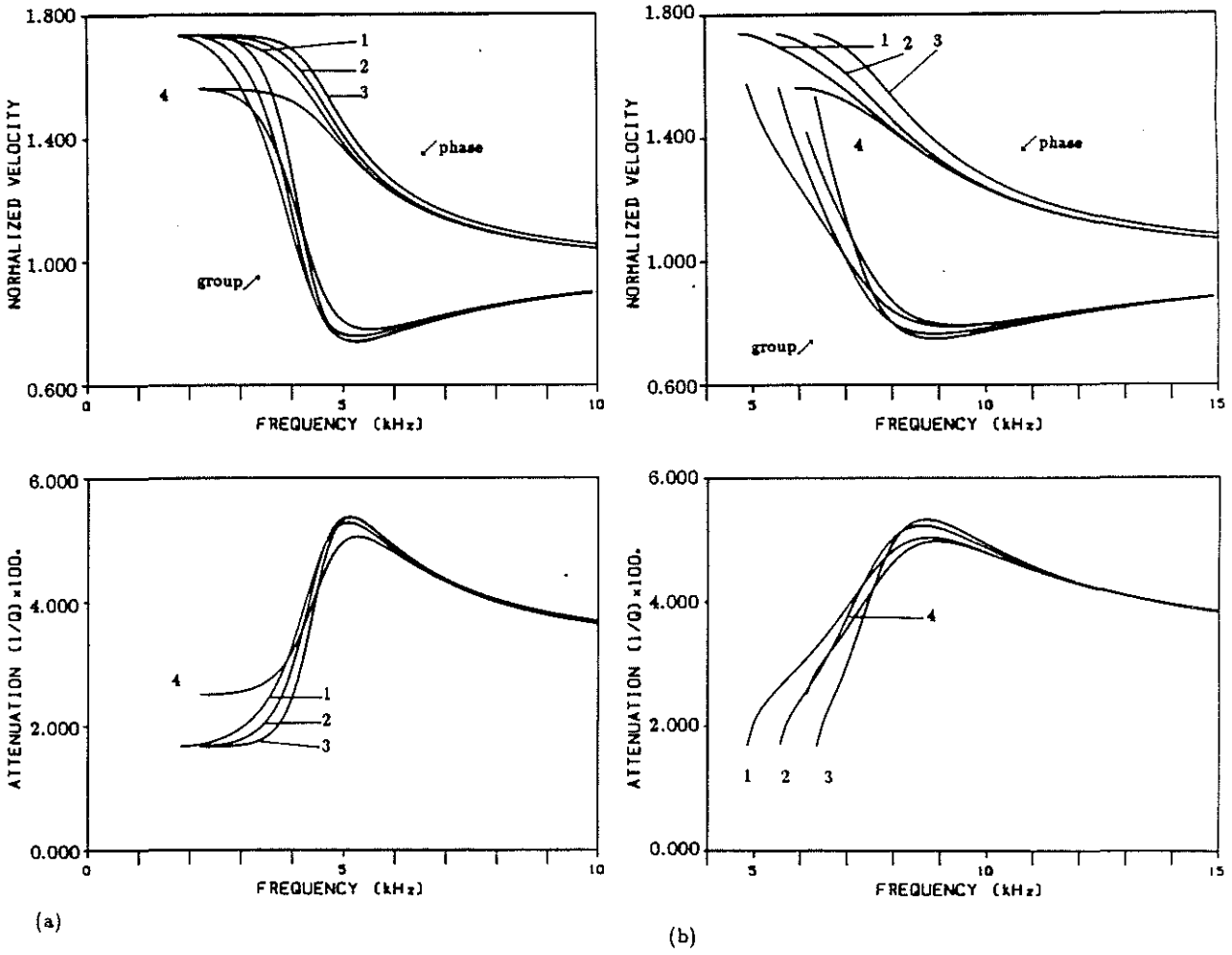

Figure 12: Invaded zone effects with a fast sandstone. Dispersion and attenuation of the flexural (a) and screw (b) modes in the presence of: (1) a 16 cm thick invaded zone; (2) a 8 cm thick invaded zone; (3) the only virgin formation ; (4) the only invaded zone. The parameters of the formations are given in Table 1. The velocities are normalized with respect to the bore fluid velocity.

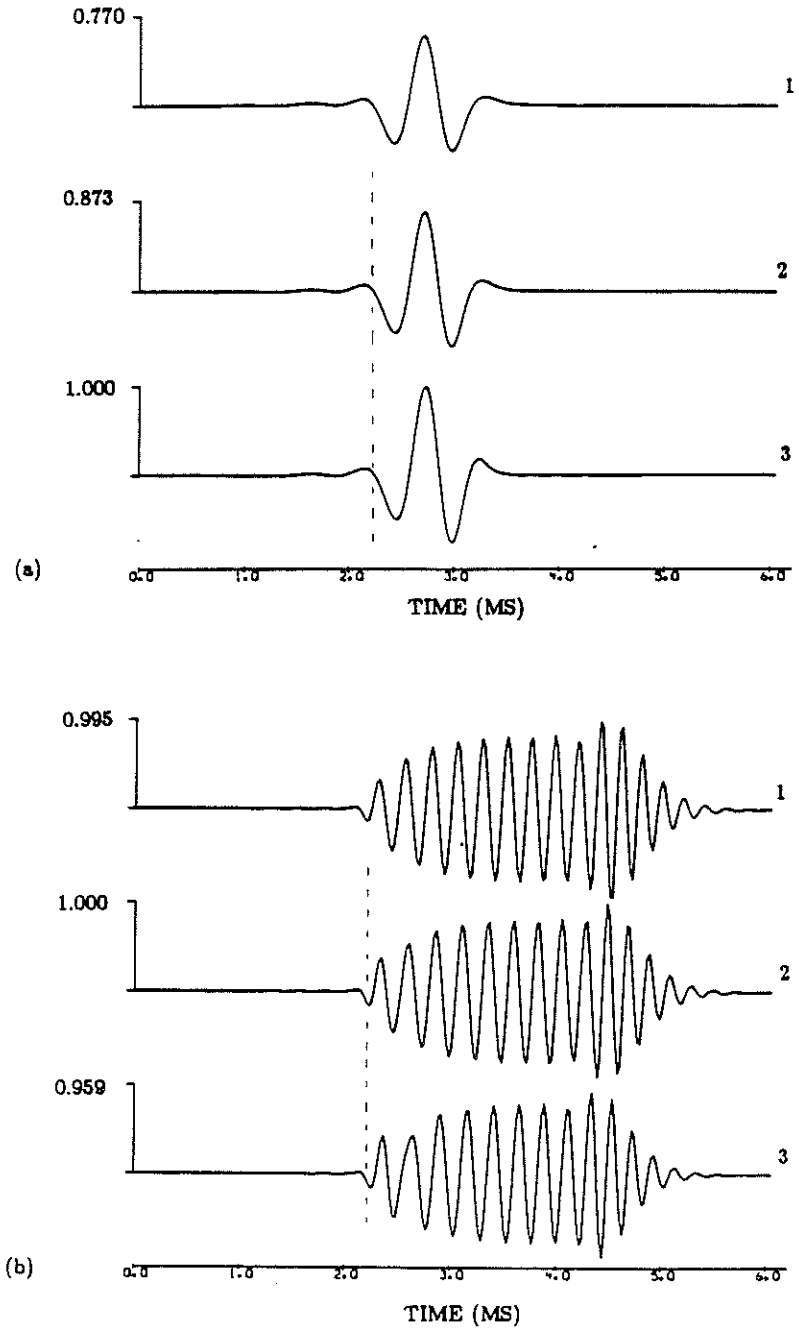

Figure 13: Dipole source. Invaded zone effects in the presence of a fast sandstone. Iso-offset (z = 5m) of the waveforms obtained in the presence of the only virgin formation (1), and a 8 cm (2) and 16 cm (3) invaded zone. The source center frequency is successively equal to 1 kHz (a), 3 kHz (b), 6 kHz (c), and 7.5 kHz (d). Each series is normalized with respect to its own maximum denoted by 1.00.

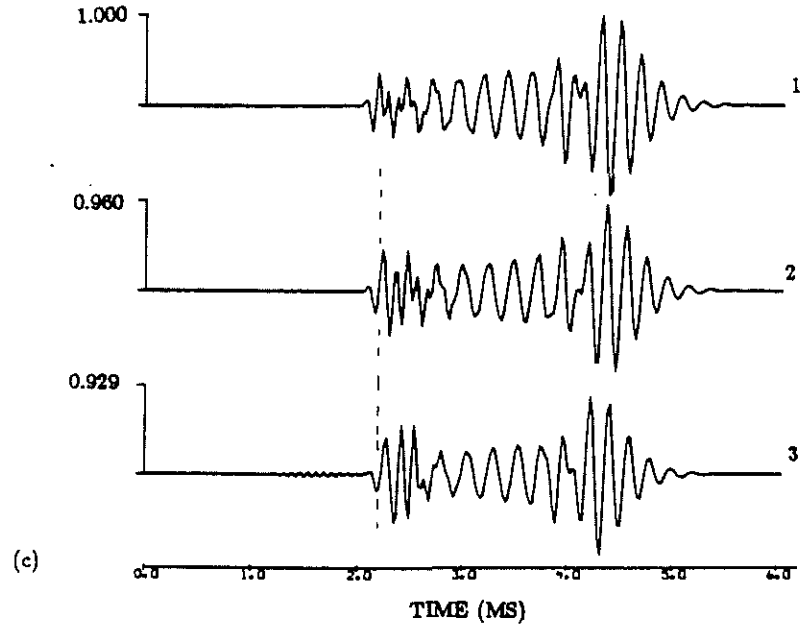

(c)

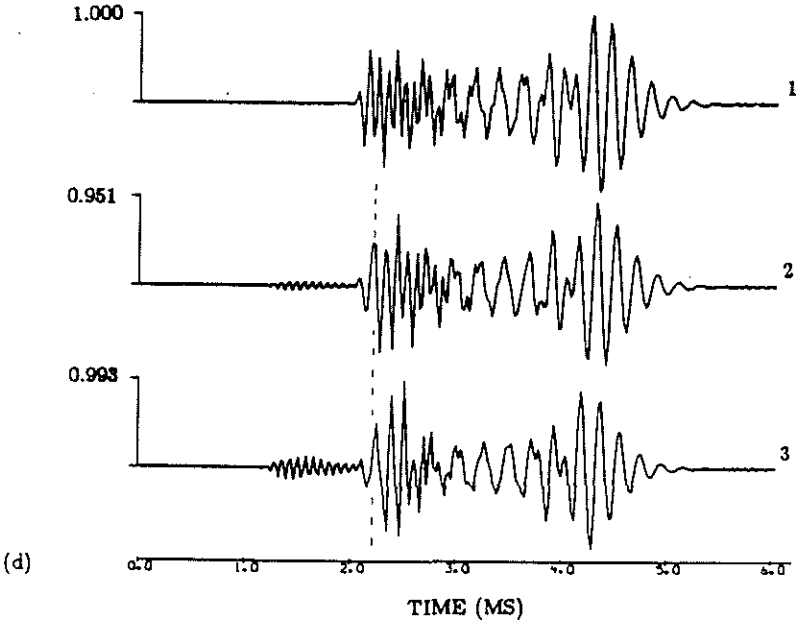

(d)

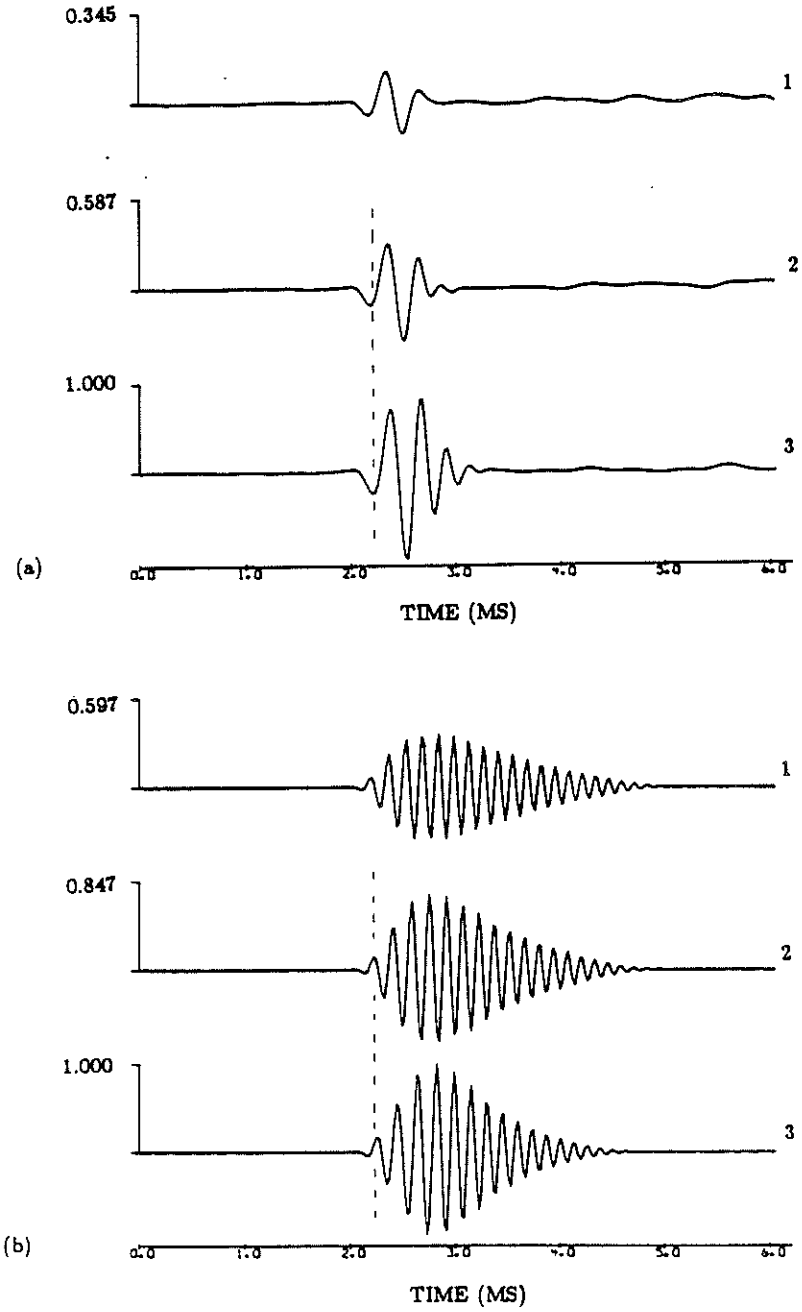

Figure 14: Quadrupole source. Invaded zone effects in the presence of a fast sandstone. Iso-offset (z = 5m) of the waveforms obtained in the presence of the only virgin formation (1), and a 8 cm (2) and 16 cm (3) invaded zone. The source center frequency is successively equal to 1.5 kHz (a), 3 kHz (b), 6 kHz (c), and 7.5 kHz (d). Each series is normalized with respect to its own maximum denoted by 1.00.

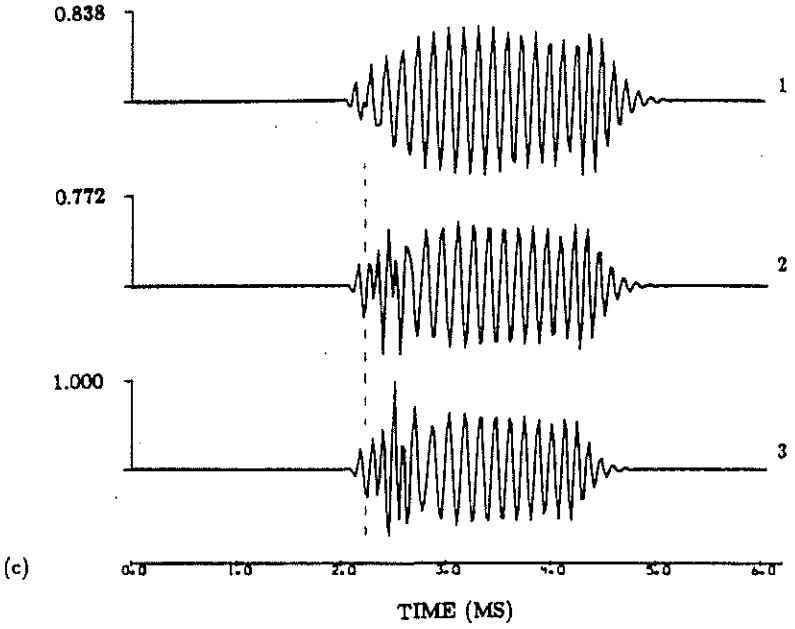
0.838
1
0.772
2
1.000
3
(c)
TIME (MS)

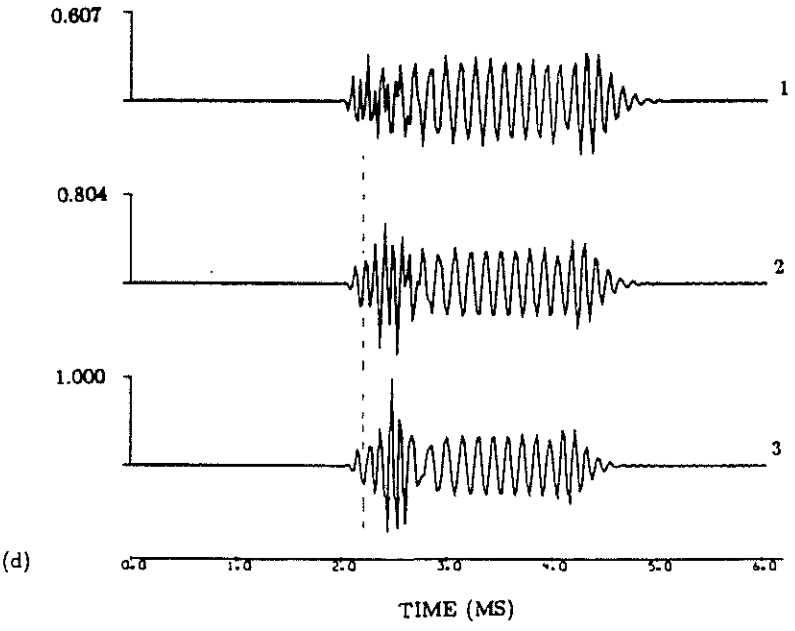
0.607
1
0.804
2
1.000
3
(d)
TIME (MS)

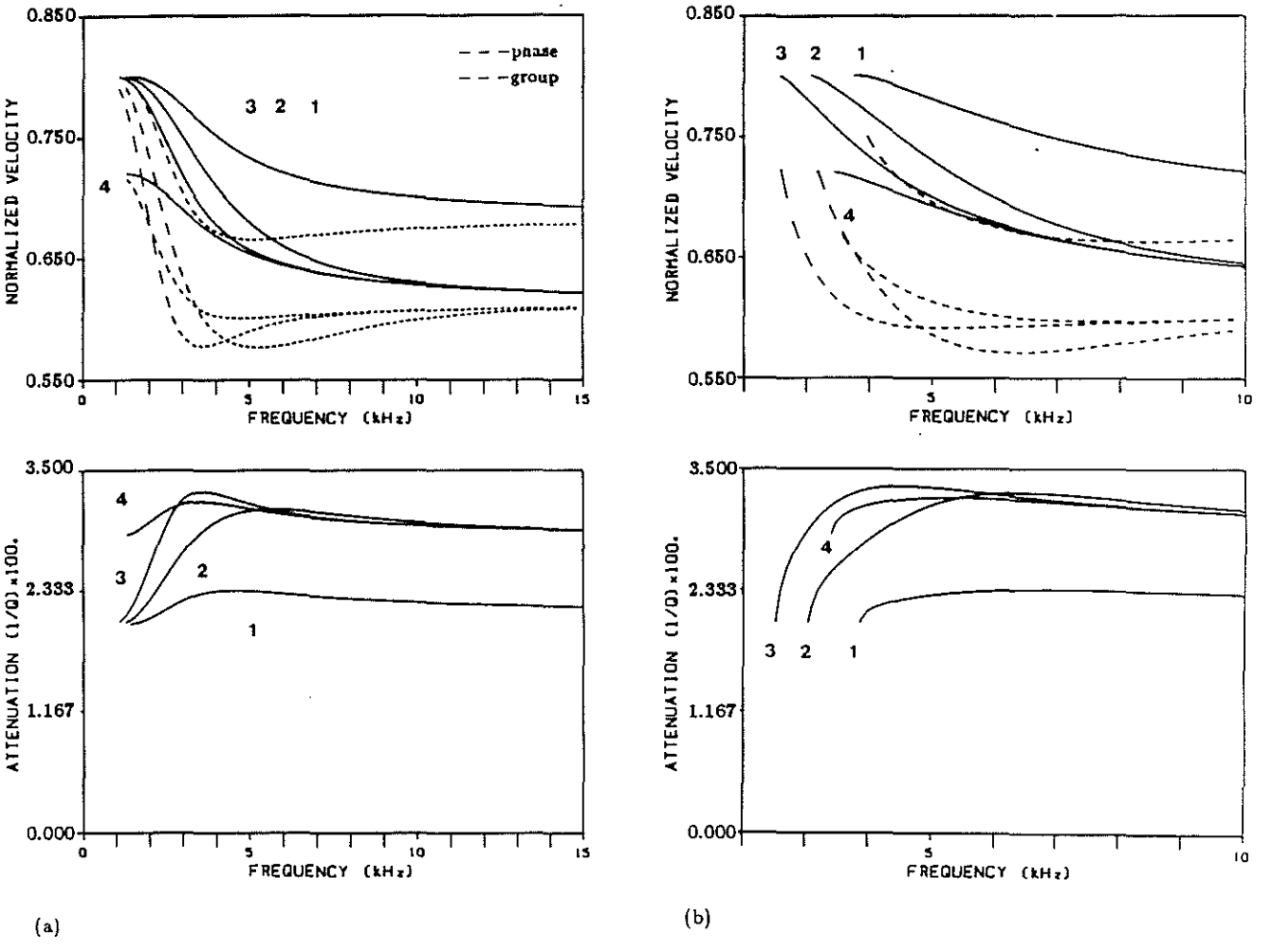

Figure 15: Invaded zone effects with a slow sandstone. Dispersion and attenuation of the flexural (a) and screw (b) modes in the presence of: (1) the only virgin formation; (2) a 8 cm thick invaded zone; (3) a 16 cm thick invaded zone; (4) the only invaded zone. The parameters of the formations are given in Table 1. The velocities are normalized with respect to the bore fluid velocity.

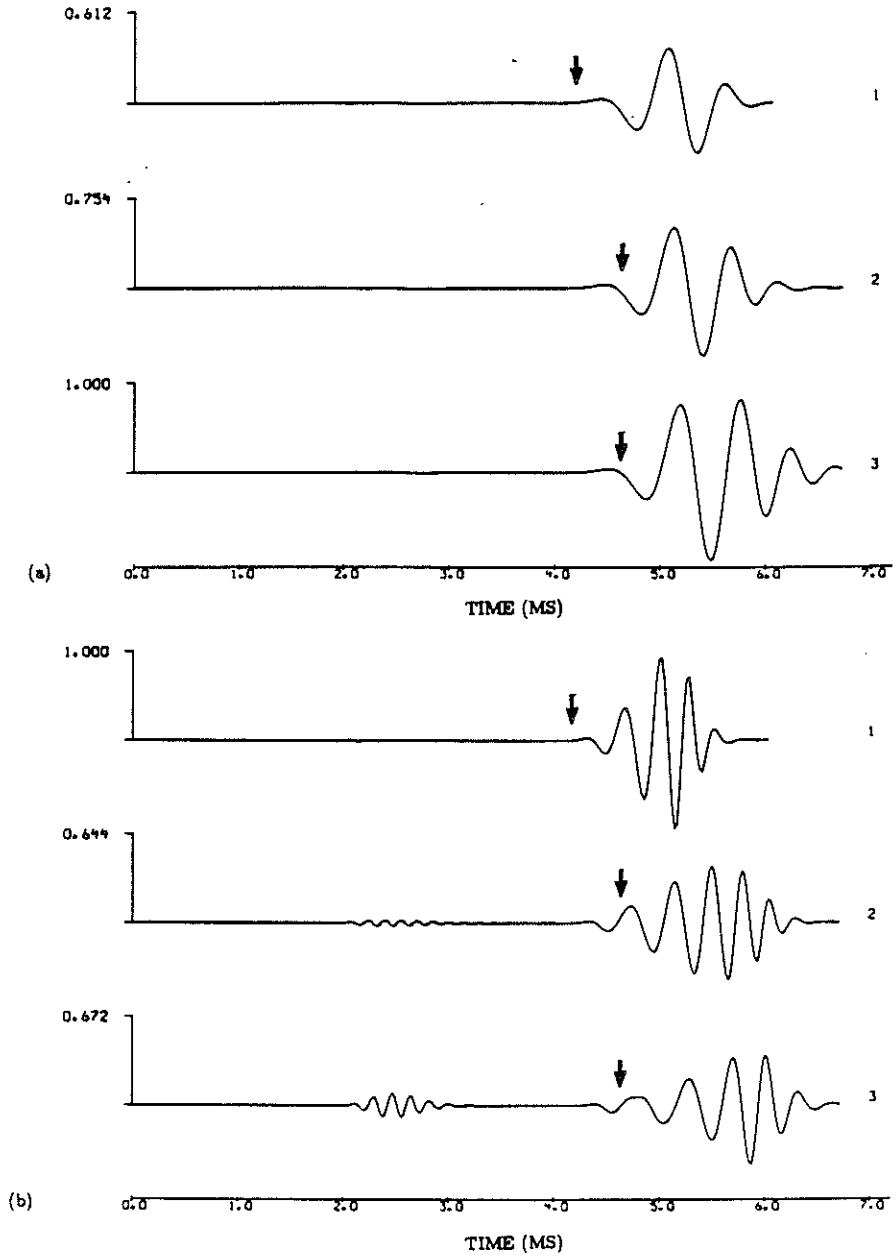

Figure 16: Dipole source. Invaded zone effects in the presence of a slow sandstone. Iso-offset ($z = 5$m) of the waveforms obtained in the presence of the only virgin formation (1), and a 8 cm (2) and 16 cm (3) invaded zone. The source center frequency is successively equal to 1 kHz (a), 3 kHz (b), 6 kHz (c), and 7.5 kHz (d). Each series is normalized with respect to its own maximum denoted by 1.00.

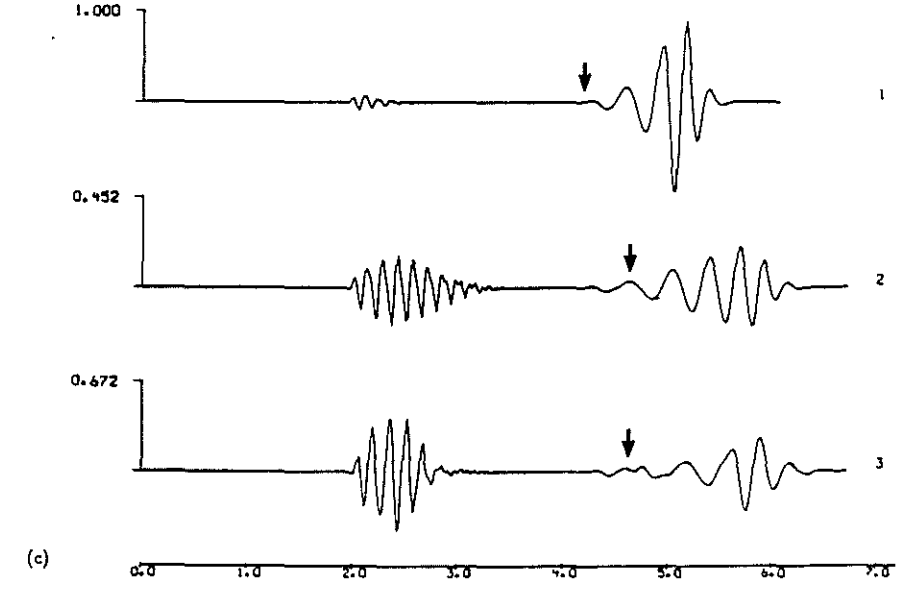
1.000
0.452
0.672
1
2
3
0.0
1.0
2.0
3.0
4.0
5.0
6.0
7.0
TIME (MS)

(c)

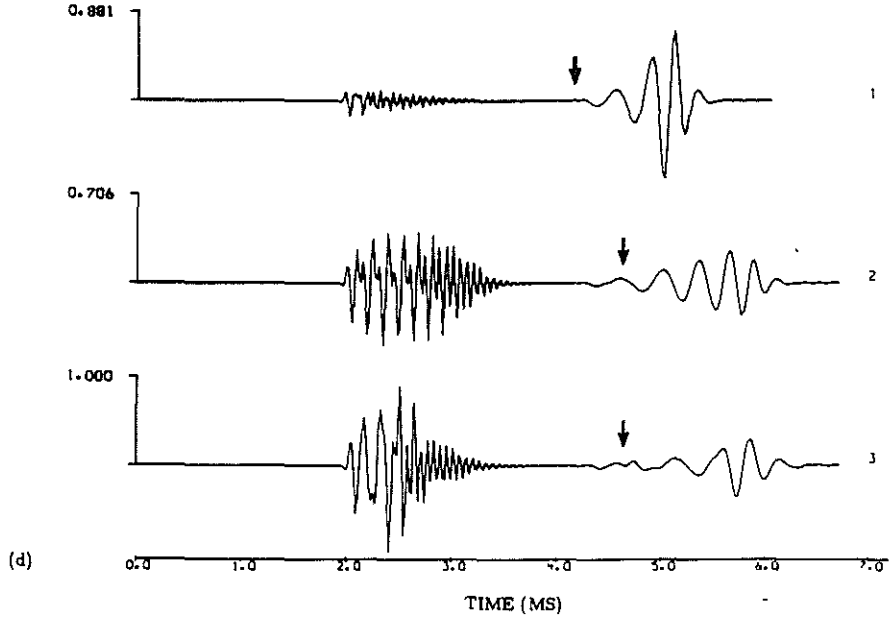
0.881
0.706
1.000
1
2
3
0.0
1.0
2.0
3.0
4.0
5.0
6.0
7.0
TIME (MS)

(d)

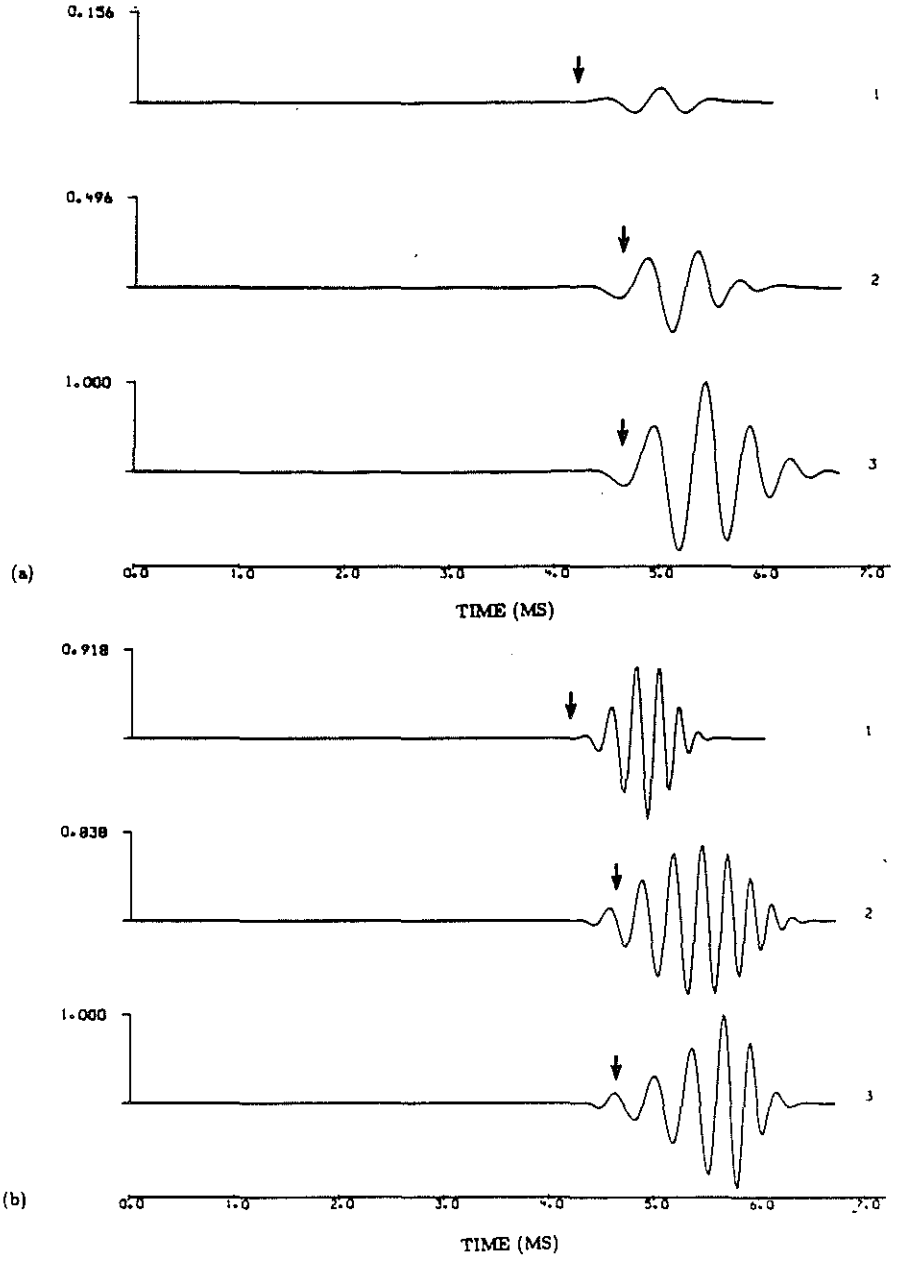

Figure 17: Quadrupole source. Invaded zone effects in the presence of a slow sandstone. Iso-offset (z = 5m) of the waveforms obtained in the presence of the only virgin formation (1), and a 8 cm (2) and 16 cm (3) invaded zone. The source center frequency is successively equal to 1 kHz (a), 3 kHz (b), 6 kHz (c), and 7.5 kHz (d). Each series is normalized with respect to its own maximum denoted by 1.00.

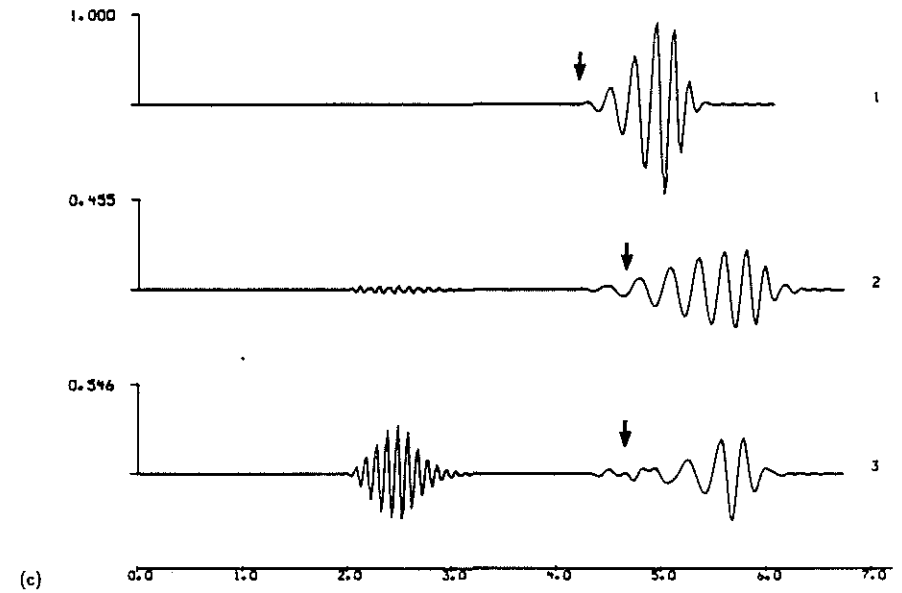
1.000
0.455
0.346
1
2
3
0.0
1.0
2.0
3.0
4.0
5.0
6.0
7.0
TIME (MS)

(c)

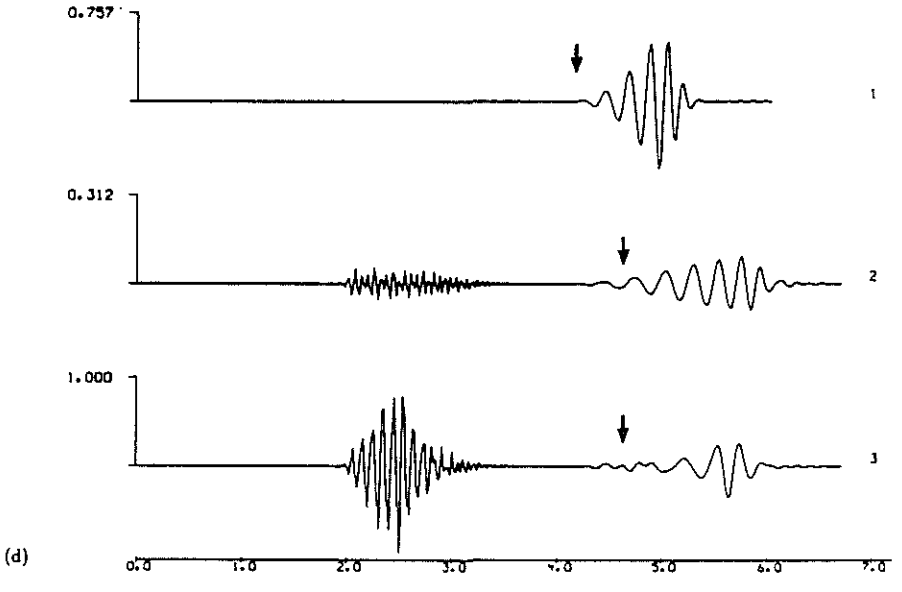
0.757
0.312
1.000
1
2
3
0.0
1.0
2.0
3.0
4.0
5.0
6.0
7.0
TIME (MS)

(d)

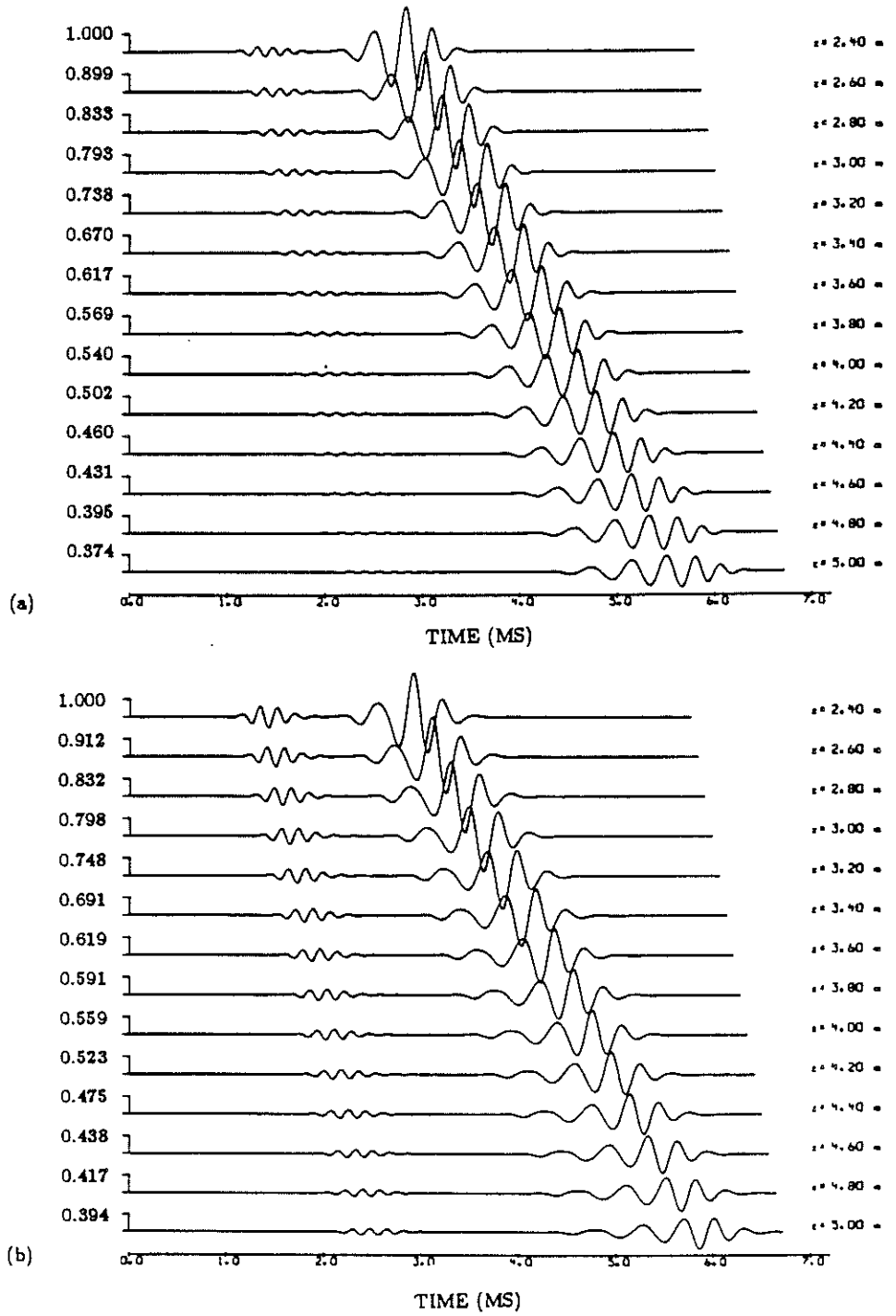

Figure 18: Dipole source, slow sandstone. Invaded zone effects. Shot points obtained with a 3 kHz source center frequency in the presence of a 8 cm (a) and 16 cm (b) invaded zone. Each series is normalized with respect to its own maximum denoted by 1.00. Compare with Figure 10a.

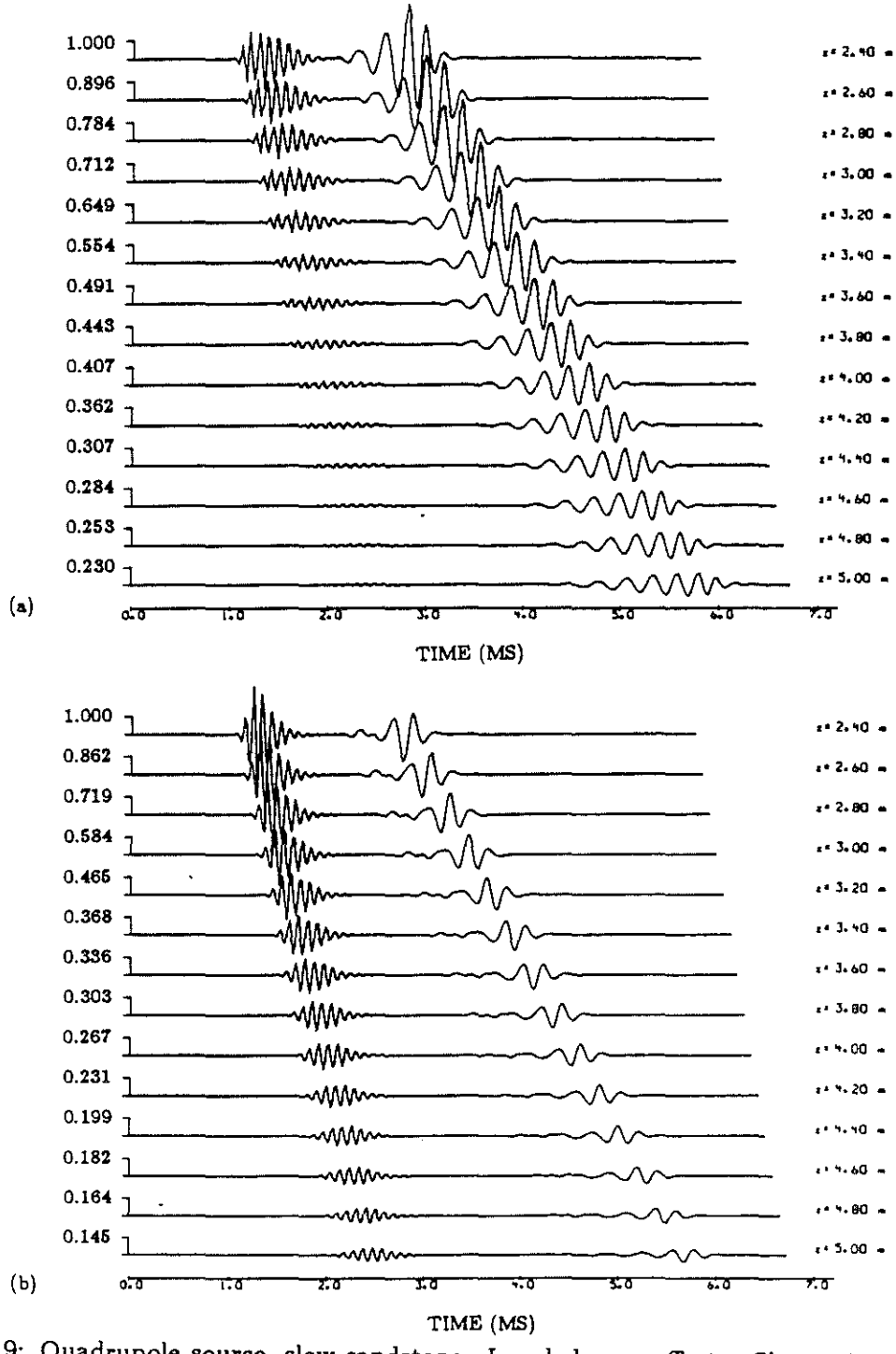

Figure 19: Quadrupole source, slow sandstone. Invaded zone effects. Shot points obtained with a 6 kHz source center frequency in the presence of a 8 cm (a) and 16 cm (b) invaded zone. Each series is normalized with respect to its own maximum denoted by 1.00. Compare with Figure 11a.

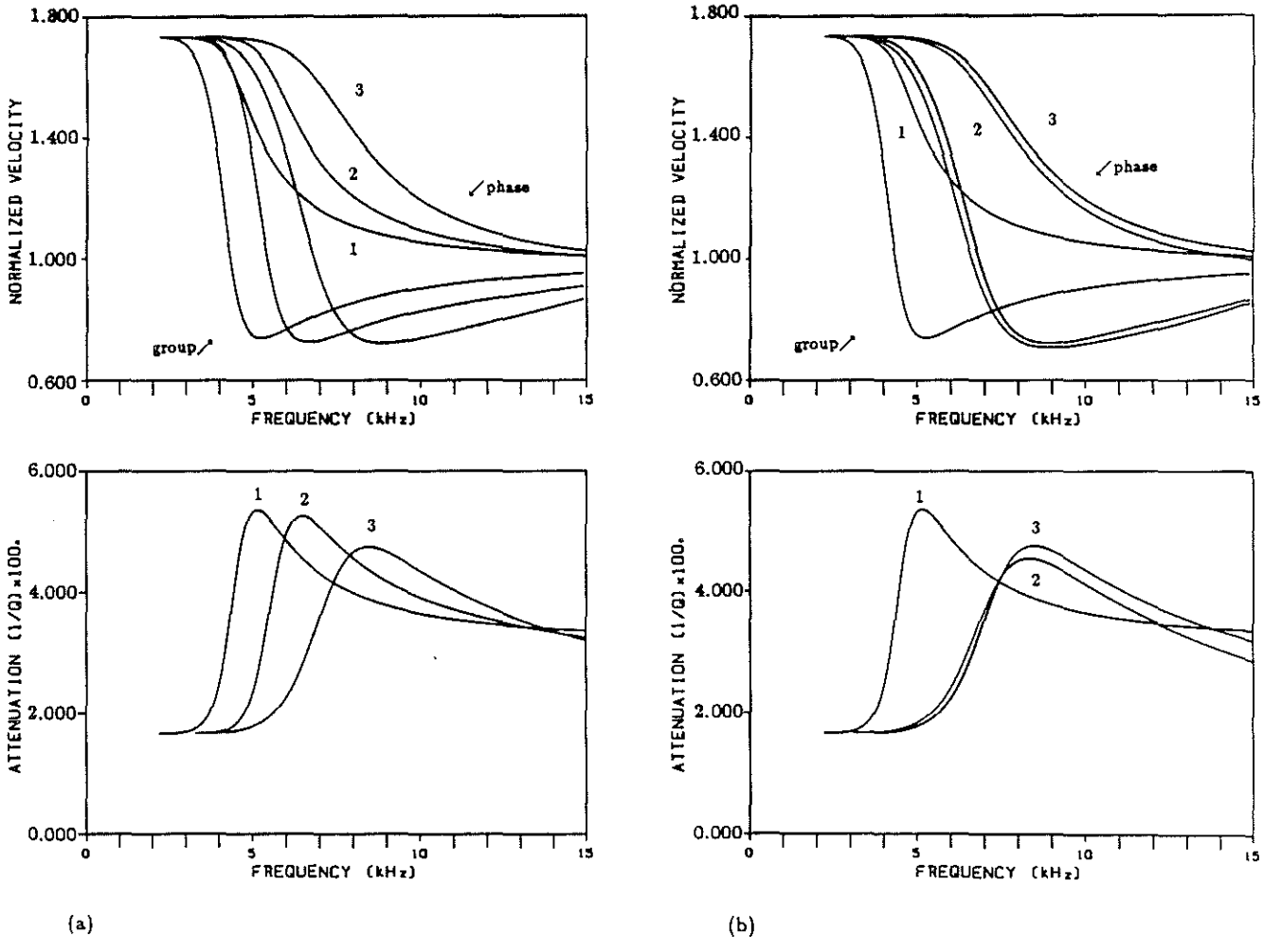

Figure 20: Dipole source. Well-bonded cased hole configuration with a fast sandstone. Dispersion and attenuation of the flexural mode. The original borehole radius is 10 cm and the steel casing is 1.02 cm thick. (a): Cement thickness effects. (1): open hole, (2): 1 cm thick cement 1, (3): 3 cm thick cement 1. (b): Cement shear velocity effects. (1): open hole, (2): cement 2, (3): cement 1. The thickness of the cement is 3 cm. The parameters of the layers are given in Table 1.

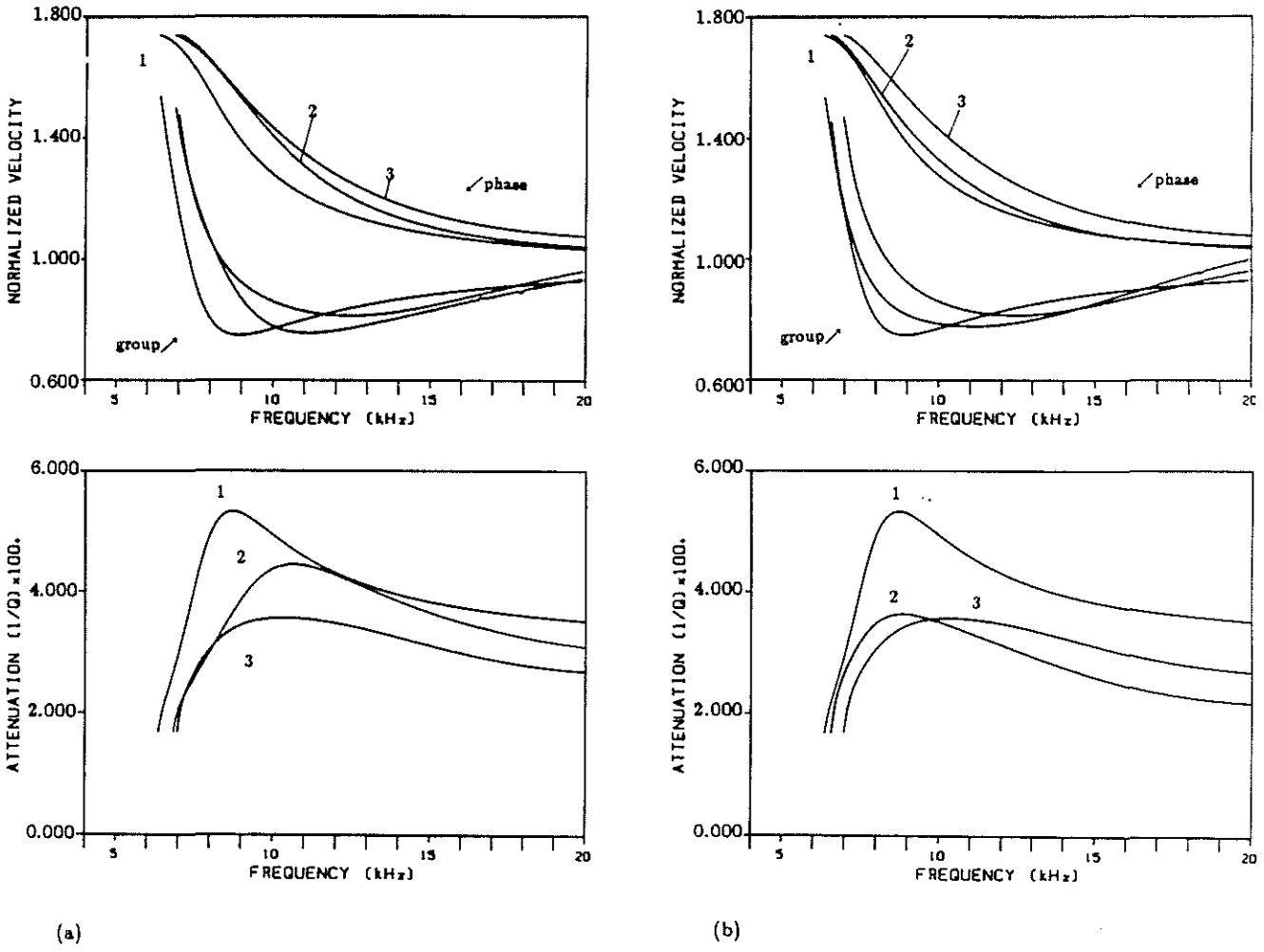

Figure 21: Quadrupole source. Same as Figure 20 for the screw mode.

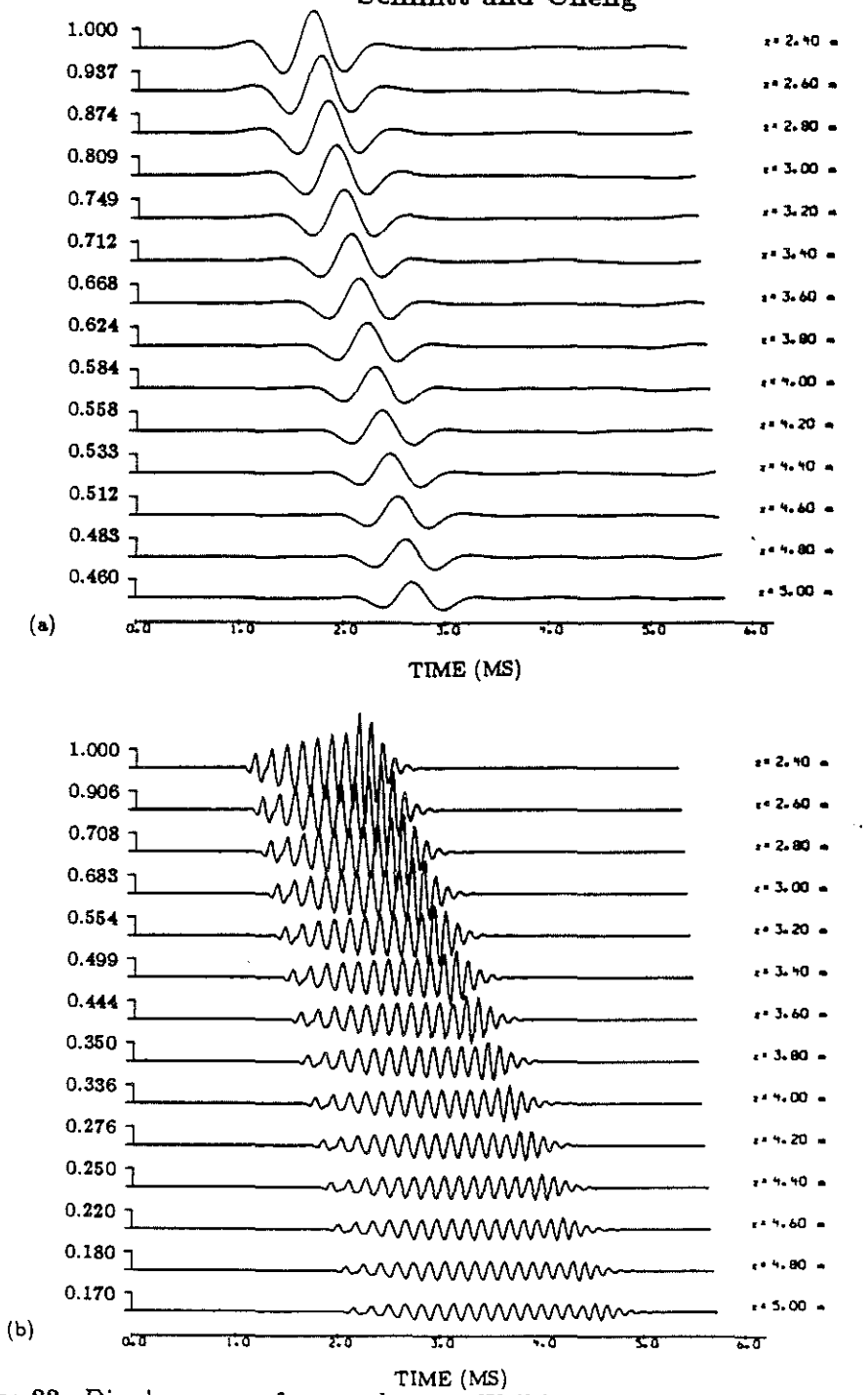

Figure 22: Dipole source, fast sandstone. Well-bonded cased hole configuration. Synthetic microseismograms associated with the case (3) of Figure 20a. Shot points obtained with a 1 kHz (a) and a 6 kHz (b) source center frequency. Each series is normalized with respect to its own maximum denoted by 1.00. Compare with Figures 4a, b, respectively.

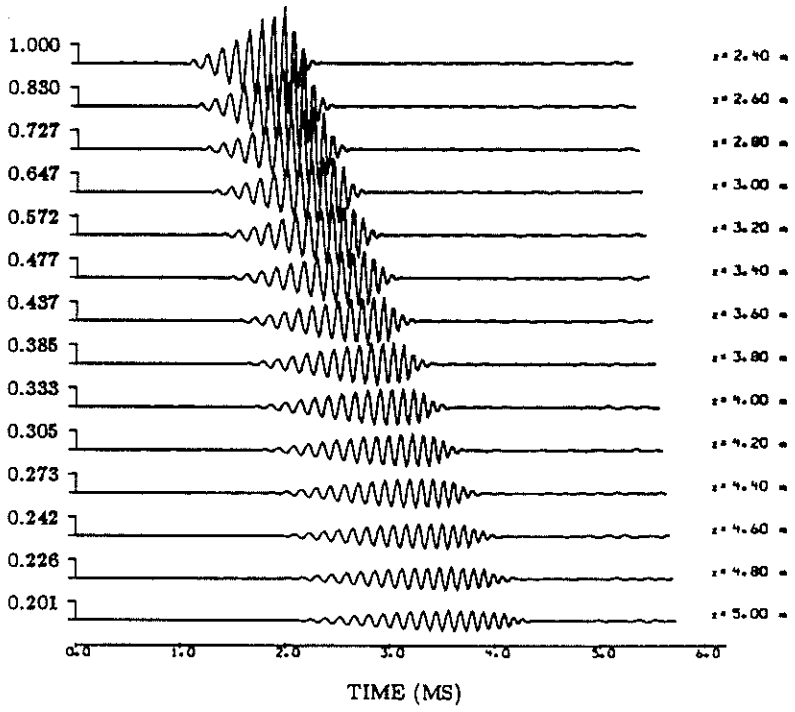

Figure 23: Quadrupole source, fast sandstone. Well-bonded cased hole configuration. Synthetic microseismograms associated with the case (3) of Figure 21a. Shot point obtained with a 6 kHz source center frequency. Each waveform is normalized with respect to the maximum of the whole series denoted by 1.00. Compare with Figure 6b.

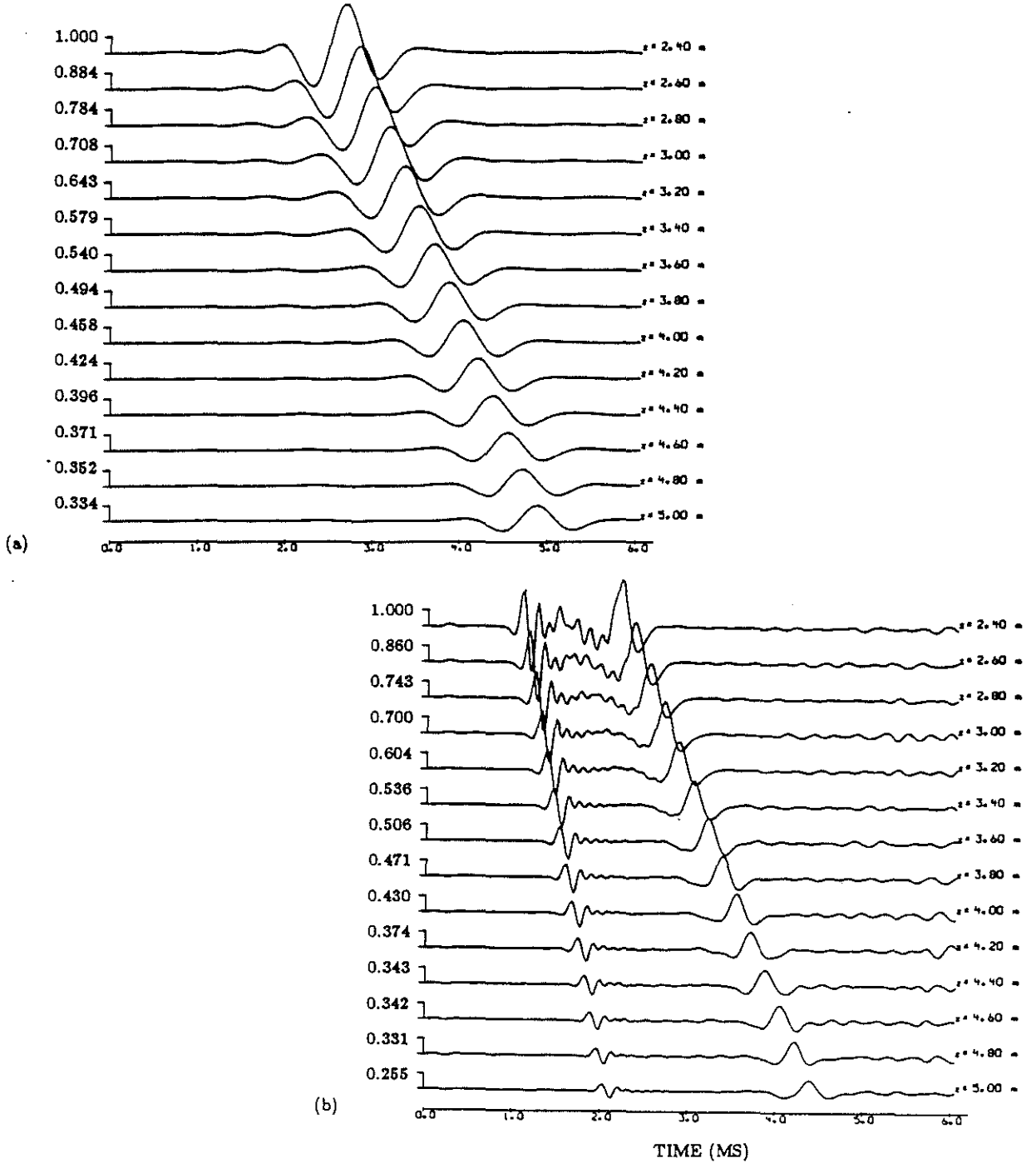

Figure 24: Dipole source, slow sandstone. Well-bonded cased hole configuration. The original borehole radius is 10 cm, the casing is 1.02 cm, and the cement layer (cement 1) is 3 cm thick. Shot points obtained with a 1 kHz (a), a 3 kHz (b), and a 6 kHz (c) source center frequency. Each series is normalized with respect to its own maximum denoted by 1.00. Compare with Figures 10a, b, respectively.

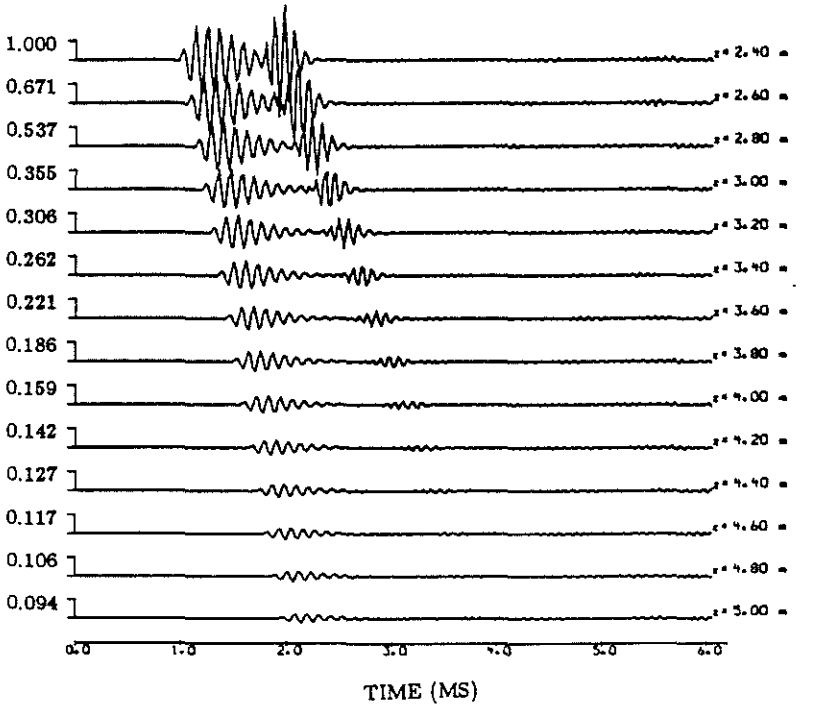
1.000
0.671
0.537
0.355
0.306
0.262
0.221
0.186
0.159
0.142
0.127
0.117
0.106
0.094
0.0
1.0
2.0
3.0
4.0
5.0
6.0
TIME (MS)

(c)

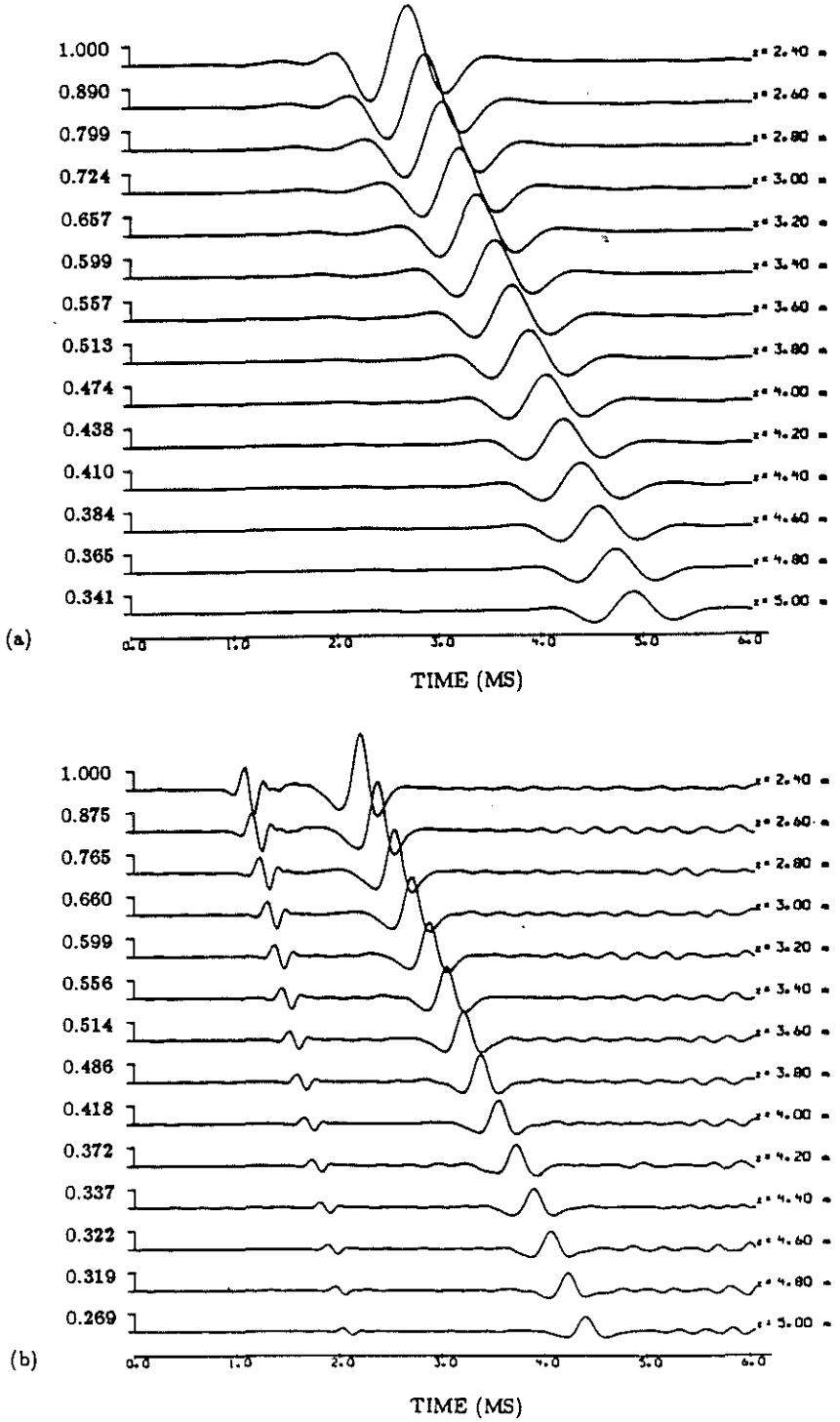

Figure 25: Dipole source, slow sandstone. Well-bonded case hole configuration. Shot points obtained when no cement is present with a 1 kHz (a) and 3 kHz (b) source center frequency. Compare with Figures 24, 10 a,b, respectively.